Update on the Temperature Corrections of Global Air-Sea CO_2 Flux Estimates

Yuanxu Dong[1], Dorothee C. E. Bakker[1], Thomas G Bell[2], Boyin Huang[3], Peter Landschützer[4], Peter S. Liss[1], and Mingxi Yang[2]

[1]University of East Anglia
[2]Plymouth Marine Laboratory
[3]NOAA/NCEI
[4]Max Planck Institute for Meteorology

November 23, 2022

Abstract

The oceans are a major carbon sink. Sea surface temperature (SST) is a crucial variable in the calculation of the air-sea carbon dioxide (CO_2;) flux from surface observations. Any bias in the SST or any upper ocean vertical temperature gradient (e.g., the cool skin effect) potentially generates a bias in the CO_2 flux estimates. A recent study suggested a substantial increase (~50% or ~0.9 Pg C yr-1) in the global ocean CO_2 uptake due to this temperature effect. Here, we use a gold standard buoy SST dataset as the reference to assess the accuracy of in-situ SST used for flux calculation. A physical model is then used to estimate the cool skin effect, which varies with latitude. The bias-corrected SST (assessed by buoy SST) coupled with the physics-based cool skin correction increases the average ocean CO_2 uptake by ~35% (0.6 Pg C yr-1) for 1982 to 2020, which is significantly smaller than the previous correction. After these temperature considerations, we estimate an average net ocean CO_2 uptake of 2.2 +- 0.4 Pg C yr-1 for 1994 to 2007 based on an ensemble of surface observation-based flux estimates, in line with the independent interior ocean carbon storage estimate corrected for the river induced natural outgassing flux (2.1 +- 0.4 Pg C yr-1).

Update on the Temperature Corrections of Global Air-Sea CO_2 Flux Estimates

Yuanxu Dong[1,2], Dorothee C. E. Bakker[1]*, Thomas G. Bell[2], Boyin Huang[3], Peter Landschützer[4], Peter S. Liss[1], Mingxi Yang[2]

[1]Centre for Ocean and Atmospheric Sciences, School of Environmental Sciences, University of East Anglia, Norwich, UK

[2]Plymouth Marine Laboratory, Prospect Place, Plymouth, UK

[3]National Centers for Environmental Information, National Oceanic and Atmospheric Administration, Asheville, NC, USA

[4]Max Planck Institute for Meteorology, Hamburg, Germany

Correspondence to: Yuanxu Dong (Yuanxu.Dong@uea.ac.uk)

*Co-corresponding author: Dorothee C. E. Bakker (D.Bakker@uea.ac.uk)

Key points:

- The impact of the warm bias in an *in-situ* SST dataset and the cool skin effect on air-sea CO_2 flux estimates are re-visited
- The updated temperature corrections imply a smaller increase in net ocean CO_2 uptake (~35%) compared to a previous study (~50%)
- The revised observation-based CO_2 flux agrees well with the independent ocean carbon inventory

Abstract

The oceans are a major carbon sink. Sea surface temperature (SST) is a crucial variable in the calculation of the air-sea carbon dioxide (CO_2) flux from surface observations. Any bias in the SST or any upper ocean vertical temperature gradient (e.g., the cool skin effect) potentially generates a bias in the CO_2 flux estimates. A recent study suggested a substantial increase (~50% or ~0.9 Pg C yr^{-1}) in the global ocean CO_2 uptake due to this temperature effect. Here, we use a gold standard buoy SST dataset as the reference to assess the accuracy of *in-situ* SST used for flux calculation. A physical model is then used to estimate the cool skin effect, which varies with latitude. The bias-corrected SST (assessed by buoy SST) coupled with the physics-based cool skin correction increases the average ocean CO_2 uptake by ~35% (0.6 Pg C yr^{-1}) for 1982 to 2020, which is significantly smaller than the previous correction. After these temperature considerations, we estimate an average net ocean CO_2 uptake of 2.2 ± 0.4 Pg C yr^{-1} for 1994 to 2007 based on an ensemble of surface observation-based flux estimates, in line with the independent interior ocean carbon storage estimate corrected for the river induced natural outgassing flux (2.1 ± 0.4 Pg C yr^{-1}).

Plain Language Summary

The global oceans play a major role in taking up carbon dioxide (CO_2) released by human activity from the atmosphere. Accurate sea surface temperature (SST) measurements and quantification of any upper ocean temperature gradients (e.g., cool skin effect) are critical for ocean CO_2 uptake estimates. We determine a slight warm bias in the SST dataset used for CO_2 flux calculation by utilizing a gold standard reference buoy SST dataset. We then derive a physics-based temperature correction for the ubiquitous cool skin effect on the ocean surface. The temperature revised CO_2 flux bridges the gap between estimates from the surface observation-based air-sea CO_2 fluxes and from the independent ocean carbon inventory.

1 Introduction

Since the Industrial Revolution, humans have emitted large amounts of carbon dioxide (CO_2) to the atmosphere, which is the main reason for observed global warming. The oceans are a major CO_2 sink accounting for ~25% (~2.5 Pg C yr^{-1} for the last decade) of the annual anthropogenic CO_2 emissions (Friedlingstein et al., 2020) and ~40% of all anthropogenic CO_2 since industrialization (Gruber et al., 2019; Sabine et al., 2004).

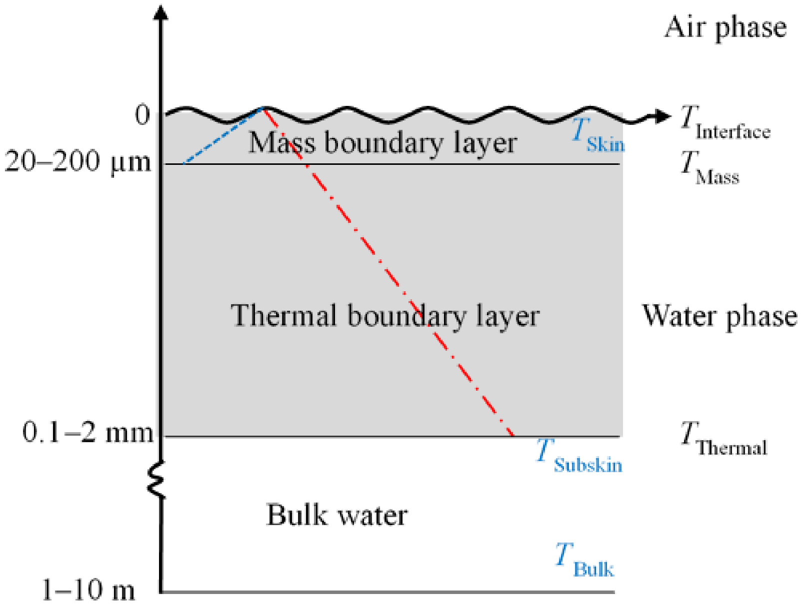

Figure 1. A schematic of the upper ocean (0–10 m depth) using an example where temperature is influenced by a positive (ocean heat loss) sensible heat flux and CO_2 is being taken up by the ocean. The grey shaded area represents the thermal boundary layer (TBL), and the red line represents the temperature gradient in the TBL. The mass (in this case, CO_2) boundary layer (MBL) is embedded within the TBL. The blue line corresponds to the CO_2 concentration gradient within the MBL. The TBL is characteristically ten times thicker than the MBL because heat is transferred about an order of magnitude quicker than CO_2 (Jähne, 2009). $T_{Interface}$: the temperature at the air-sea interface; T_{Skin}: the skin temperature at ~10 μm depth measured by an infrared radiometer; T_{Mass}: the temperature at the base of the MBL (20–200 μm depth); $T_{Thermal}$: the temperature at the base of the TBL (0.1–2 mm depth); $T_{Subskin}$: the temperature of seawater below the TBL at a depth of ~0.1–1 m such as measured by drifting buoys; T_{Bulk}: the temperature at 1–10 m depth as measured at the typical depth of a ship's seawater intake. $T_{Interface}$, T_{Mass}, and $T_{Thermal}$ are conceptual, whereas T_{Skin}, $T_{Subskin}$, and T_{Bulk} are from actual measurements (practical). Sea surface temperature (SST) is a general term for all temperatures mentioned above. Figure developed from Donlon et al. (2007).

The global air-sea CO_2 flux is often estimated by the bulk method combining *in-situ* fCO_{2w} (fugacity of CO_2 in seawater) measurements (e.g., from the Surface Ocean CO_2 Atlas, SOCAT; Bakker et al., 2016) with a wind speed-dependent gas transfer velocity (e.g., Wanninkhof, 2014; see Methods). Thanks to the SOCAT (http://www.socat.info/) community, a key dataset of

fCO_{2w} has been available since 2011 (Pfeil et al., 2013; Sabine et al., 2013). The latest SOCAT version, SOCAT v2021, contains 30.6 million quality-controlled fCO_{2w} observations from 1957 to 2020 with an accuracy better than 5 µatm (Bakker et al., 2016, 2021).

Sea surface temperature (SST) is key for bulk air-sea CO_2 flux estimates. Takahashi et al. (2009) reported a 13% increase in ocean CO_2 uptake by correcting for a 0.08 K warm bias in SST. CO_2 is a water-side controlled gas (Liss & Slater, 1974), and thus air-sea CO_2 exchange is mainly limited by transfer within the ~20–200 µm mass boundary layer (MBL, Figure 1; Jähne, 2009). The MBL temperature should be used for the CO_2 flux calculation, but it is impractical to measure *in-situ* SST within the very thin MBL. The bulk *in-situ* seawater temperature (T_{Bulk}) measured concurrently with fCO_{2w} (typically at ~5 m depth) in SOCAT is often used for the bulk air-sea CO_2 flux calculation by assuming a well-mixed upper ocean (top ~10 m) without any vertical temperature gradients.

However, there are two issues with using the SOCAT SST. Firstly, many processes can generate vertical temperature gradients in the upper ocean. There is a temperature gradient (red line in Figure 1) in the thermal boundary layer (TBL, grey shaded area) relating to air-sea heat exchange. Infrared radiometer measurements indicate that the skin temperature at ~10 µm depth (T_{Skin}) is on average ~0.17 K (Donlon et al., 2002) lower than the subskin temperature ($T_{Subskin}$, at ~0.1–1 m depth) because the ocean surface generally loses heat through longwave radiation, and latent and sensible heat fluxes (the so-called cool skin effect; e.g., Donlon et al., 2007, 2002; Minnett et al., 2011; Robertson & Watson, 1992; Zhang et al., 2020). Another process that might create an upper ocean temperature gradient is the diurnal warm layer effect. Water close to the surface (e.g., at 0.5 m depth) is sometimes warmer than deeper water (e.g., at 5 m depth) due to daytime solar insolation, especially under conditions of clear sky and low wind speed (Gentemann & Minnett, 2008; Prytherch et al., 2013; Ward et al., 2004). The warming leads to stabilization of the surface layer and thus helps maintain a layered upper ocean structure. The diurnal warm layer effect is not as ubiquitous as the cool skin effect, and the warm layer is complex to characterize. In the absence of the warm layer effect, the bulk seawater temperature (T_{Bulk}) is approximately equal to $T_{Subskin}$, and $T_{Thermal}$ (temperature at the base of the TBL) because the water below the TBL is well-mixed by turbulence.

The second issue is the potential warm bias in the SOCAT SST. The SST community has identified a warm bias in shipboard SST measurements in the ICOADS (International Comprehensive Ocean-Atmosphere Data Set; Huang et al., 2021; Kennedy et al., 2011, 2019;

Reynolds & Chelton, 2010). This might be because ship SST measurements are affected by engine room warming (Kennedy et al., 2019). The SSTs in SOCAT were almost exclusively measured by shipboard systems (98%), meaning that a warm bias could also exist in the SOCAT SST dataset.

Satellite observation of SST represents a consistent estimate of subskin temperature and avoids the diurnal warm layer effect and any potential warm bias issue. Satellite SST thus has been proposed as an alternative to calculate the bulk air-sea CO_2 flux (Goddijn-Murphy et al., 2015; Shutler et al., 2019; Watson et al., 2020; Woolf et al., 2016). Results, based on a satellite SST dataset suggest a ~25% increase (i.e., warm bias correction; cool skin correction results in another ~25% increase) in ocean CO_2 uptake compared to the flux estimate based on the SOCAT SST (Watson et al., 2020). However, satellite SST is not measured concurrently with the fCO_{2w}. Co-locating the 1° × 1°, monthly gridded satellite SSTs with individual fCO_{2w} in SOCAT might introduce extra uncertainties. In addition, various issues in satellite SSTs (e.g., cloud masking, impact of aerosol, diurnal variability, uncertainty estimation, and validation) have not been fully resolved, especially at high latitudes and in coastal and highly dynamic regions (O'Carroll et al., 2019). A comparison of eight global gap-free satellite/blended SST products showed that their global mean ranged from 20.02 °C to 20.17 °C for the period 2003–2018 (at a 95% confidence level; Yang et al., 2021).

SST observations from drifting buoys are unaffected by engine room warming, and are expected to provide the best-quality reference temperature to assess bias in the ship SST, and satellite SST retrievals (Huang et al., 2021; Kennedy et al., 2011, 2019; Kent et al., 2017; Merchant et al., 2019; Reynolds & Chelton, 2010). This work utilizes drifting buoy SST as the reference temperature to determine the accuracy of the SOCAT SST, and to correct for any bias in the SOCAT SST dataset.

Subskin temperature with a cool skin correction represents the skin temperature, which can be used to calculate air-sea CO_2 flux. Watson et al. (2020) reported a ~25% increase in ocean CO_2 uptake by considering a constant cool skin effect (-0.17 K, Donlon et al., 2002) for 1982 to 2020. In this study, the cool skin effect estimated by a physical model (Fairall et al., 1996) and by an empirical model (Donlon et al., 2002) are compared at a global scale. The updated temperature corrections are then used to estimate their impact on the global air-sea CO_2 flux. The revised global air-sea CO_2 flux based on an ensemble of CO_2 flux products (Fay et al., 2021) is then compared with the ocean carbon inventory (Gruber et al., 2019).

2 Methods

2.1 Global Air-Sea CO_2 Flux Estimates

The bulk air-sea CO_2 flux equation is:

$$F = K_{660}(Sc/660)^{-0.5}(\alpha_w f\mathrm{CO}_{2\mathrm{w}} - \alpha_i f\mathrm{CO}_{2\mathrm{a}}) \quad (1)$$

where F (mmol m^{-2} day^{-1}) is the air-sea CO_2 flux and K_{660} (cm h^{-1}) is the gas transfer velocity (e.g., Wanninkhof, 2014) normalized to a Sc (Schmidt number) of 660. The Sc is defined as the ratio of the kinematic viscosity of water (m^2 s^{-1}) and the molecular diffusivity of CO_2 (m^2 s^{-1}). The CO_2 solubility (mol L^{-1} atm^{-1}) at the base of the MBL and at the air-sea interface are represented by α_w and α_i, respectively (Figure 1). Sc and α are calculated from seawater temperature and salinity (Wanninkhof et al., 2009; Weiss, 1974). Sc is equal to 660 for CO_2 at 20 °C and 35 psu seawater. The CO_2 fugacity (µatm) at the base of the MBL and just above the air-sea interface are represented by $f\mathrm{CO}_{2\mathrm{w}}$ and $f\mathrm{CO}_{2\mathrm{a}}$, respectively.

To calculate the global air-sea CO_2 flux, $f\mathrm{CO}_{2\mathrm{w}}$ measured at the equilibrator temperature is first corrected to the *in-situ* bulk temperature (SOCAT SST). Seawater at ~5 m depth (ranging from 1–10 m depth) is sampled from the ship's underway water intake and is pumped through an equilibrator. The equilibrated CO_2 mole fraction in the air of the headspace ($\chi\mathrm{CO}_{2\mathrm{w}}$) is measured in a gas analyzer. $\chi\mathrm{CO}_{2\mathrm{w}}$ is then converted to equilibrator fugacity ($f\mathrm{CO}_{2\mathrm{w\_equ}}$) (Text S1 in Supporting Information S1). $f\mathrm{CO}_{2\mathrm{w\_equ}}$ is further corrected by the chemical temperature normalization (Takahashi et al., 1993) to obtain $f\mathrm{CO}_{2\mathrm{w}}$ in the bulk seawater:

$$f\mathrm{CO}_{2\mathrm{w}} = f\mathrm{CO}_{2\mathrm{w\_equ}}\, e^{0.0423(T_{\mathrm{w\_bulk}} - T_{\mathrm{equ}})} \quad (2)$$

where $T_{\mathrm{w\_bulk}}$ is the seawater temperature measured concurrently with $f\mathrm{CO}_{2\mathrm{w}}$ at the ship's water intake at typically 5 m depth. Seawater $f\mathrm{CO}_{2\mathrm{w}}$ measurements are then interpolated to obtain a global gap-free $f\mathrm{CO}_{2\mathrm{w}}$ product (at 1° × 1°, monthly resolution, e.g., Landschützer et al., 2013). A global gap-free SST dataset is generally one of the independent input variables for the $f\mathrm{CO}_{2\mathrm{w}}$ interpolation process. Other variables in Equation 1 are calculated using a global gap-free SST product and related datasets (e.g., mole fraction of atmospheric CO_2 for the calculation of $f\mathrm{CO}_{2\mathrm{a}}$). Finally, globally mapped $f\mathrm{CO}_{2\mathrm{w}}$, $f\mathrm{CO}_{2\mathrm{a}}$, Sc, α_w, α_i, and gas transfer velocity (K_{660}, estimated using a global gap-free wind speed dataset) are used for the CO_2 flux calculation via Equation 1.

Table 1. Variables and relevant sea surface temperature (SST) types for global air-sea CO_2 flux estimates and their relative importance for the flux estimate (after Woolf et al., 2016). The back-of-the-envelope calculation in the last column is for fCO_{2w} of ~380 µatm, fCO_{2a} of ~390 µatm, and ΔfCO_2 of -10 µatm, values typical for the last decade (Landschützer et al., 2020).

Variable (x)	**Conceptual SST**	**Practical SST product**	$\frac{\partial \ln(x)}{\partial T}$	$\frac{\partial \ln(flux)}{\partial T}$
$Sc^{-0.5}$	T_{Bulk}	Global gap-free $T_{Subskin}$	2.5% K^{-1}	2.5% K^{-1}
α_i	$T_{Interface}$	T_{Skin} (Global gap-free $T_{Subskin}$ with a cool skin correction)	-2.5% K^{-1}	100% K^{-1}
fCO_{2a}	$T_{Interface}$	T_{Skin} (Global gap-free $T_{Subskin}$ with a cool skin correction)	-0.2% K^{-1}	10% K^{-1}
α_w	$T_{Thermal}$	Global gap-free $T_{Subskin}$	-2.5% K^{-1}	-100% K^{-1}
Individual fCO_{2w}	$T_{Thermal}$	Individual $T_{Subskin}$ (*In-situ* T_{Bulk} with any bias correction)	4.23% K^{-1}	160% K^{-1}
Mapped fCO_{2w}	$T_{Thermal}$	Global gap-free $T_{Subskin}$	< 4.23% K^{-1}*	< 160% K^{-1}*

*The interpolation method (e.g., MPI-SOMFFN neural network technique; Landschützer et al., 2013) can largely dampen the effect of SST on mapped fCO_{2w}.

Table 1 summarizes the SST types that should be used to calculate variables in Equation 1. Sc should be calculated from the temperature utilized to derive K_{660} (e.g., T_{Bulk} for the K_{660} derived from the dual-tracer method; e.g., Ho et al., 2006; Nightingale et al., 2000). The air-sea interface temperature ($T_{Interface}$) should be used for the calculation of fCO_{2a} and α_i, while the temperature at the base of the MBL (T_{Mass}) should be employed to calculate fCO_{2w} (via Equation 2) and α_w. However, Woolf et al. (2016) suggested that $T_{Thermal}$ might be a better temperature for calculating fCO_{2w} and α_w. The seawater carbonate system creates a unique situation for air-sea CO_2 exchange, which does not exist for other gases. Seawater temperature changes cause chemical repartitioning of the carbonate species (CO_2, carbonic acid, bicarbonate, and carbonate; Zeebe & Wolf-Gladrow, 2001). We find that the timescale of this repartitioning equilibration (e-folding time > 10 s for typical seawater; Johnson, 1982; Zeebe & Wolf-Gladrow, 2001) is much longer than the timescale (~1 s) of water mixing below the MBL but within the TBL, where viscous dissipation dominates the water mixing (Jähne, 2009; Jähne et al., 1987; Woolf et al., 2016). The explanation of the timescales is detailed in Text 2 in Supporting Information S1. Although there is a temperature gradient in the TBL due to the cool skin effect, the carbonate species are not expected to have time to thermally adjust, which suggests that T_{Thermal} is the optimal temperature for calculating fCO_{2w} and α_w.

T_{Thermal}, T_{Mass}, and $T_{\text{Interface}}$ are conceptual temperatures, which can be approximated by practical temperatures (Figure 1). Satellite SST, which represents the subskin temperature, is a good approximation for T_{Thermal} (Shutler et al., 2019; Watson et al., 2020; Woolf et al., 2016). A satellite T_{Subskin} product can be used to calculate α_w and Sc, and to map fCO_{2w} for the global ocean. T_{Subskin} with a cool skin correction can then be utilized to calculate global fCO_{2a}, and α_i. *In-situ* T_{Subskin} should ideally be used to correct fCO_{2w} from the equilibrator temperature to the subskin seawater temperature. However, the *in-situ* temperature measured concurrently with the fCO_{2w} in SOCAT is T_{Bulk}, and *in-situ* T_{Subskin} measurements are unavailable to exactly match the SOCAT space and time-stamp. Using *in-situ* T_{Bulk} (i.e., SOCAT SST) to correct fCO_{2w} is reasonable in the absence of a warm layer effect, but it is important to account for the potential warm bias in the SOCAT SST.

Table 1 also summarizes the influence of SST and the corresponding importance for the variables used to make air-sea CO_2 flux estimates (after Woolf et al., 2016). The Sc and fCO_{2a} variations due to the bias in the SST product have a small influence on the global air-sea CO_2 flux. However, any bias in the SST data used for the calculation of α_w, α_i, and especially fCO_{2w} can result in a considerable bias in the flux. The temperature influence on the fCO_{2w} mapping should be significantly dampened by the interpolation process. The most significant influence on the CO_2 flux due to temperature bias comes from individual fCO_{2w} (~160% K^{-1}, Table 1). An average bias of 0.1 K could results in a bias in fCO_{2w} of ~1.6 µatm, which corresponds to ~16% of the net air-sea CO_2 flux for the last decade (Landschützer et al., 2020).

The skin temperature should be used for the calculation of α_i and fCO_{2a}. The T_{Skin} can be obtained from T_{Subskin} with a cool skin correction. If T_{Subskin} is used rather than T_{Skin} for the calculation of α_i, and fCO_{2a}, the ocean CO_2 uptake is in theory underestimated by ~19% for the last decade with a mean cool skin effect of 0.17 K (Donlon et al., 2002).

2.2 Bias Assessment

The *in-situ* bulk SST in SOCAT is generally used to correct individual fCO_{2w} observations from the equilibrator temperature to the seawater temperature (e.g., studies in Table S1 in

Supporting Information S1). However, a warm bias might exist in the SOCAT SST due to heating in the engine room. Watson et al. (2020) co-located the DOISST v2.0 (NOAA Daily Optimum Interpolation SST dataset; Reynolds et al., 2007) with individual *in-situ* SST measurements in SOCAT. They found that the SOCAT SST is on average 0.13 ± 0.78 K higher than the co-located DOISST v2.0. However, Huang et al. (2021) pointed out that there might be a cold bias in the DOISST v2.0 and DOISST v2.1 products (the difference between DOISST v2.0 and v2.1 can be seen in Text S4 in Supporting Information S1) .

This study uses accurate SST observed by drifting buoys to assess the potential cold bias in the DOISST v2.1 and the warm bias in SOCAT SST. A drifting buoy SST dataset from iQuam (*in situ* SST Quality Monitor v2.10; Xu & Ignatov, 2014) with high accuracy (quality level = 5) is used for the assessment. The buoy SST is first gridded (1° × 1°, monthly) and then compared with the resampled DOISST v2.1 (1/4° × 1/4°, daily data are resampled to 1° × 1°, monthly resolution) and the gridded SST (1° × 1°, monthly) in SOCAT v2021.

2.3 Cool Skin Effect Estimate

The cool skin effect is ubiquitous in the ocean (Donlon et al., 2002) and should be considered when estimating air-sea CO_2 fluxes. Watson et al. (2020) used a constant value (-0.17 K) to account for the impact of the cool skin effect on air-sea CO_2 fluxes. However, the cool skin effect is affected by many environmental processes. Donlon et al. (2002) proposed a wind speed-dependent cool skin effect based on skin and bulk temperature measurements (Donlon02, hereafter). A physical model for the cool skin effect proposed by Saunders (1967) and developed by Fairall et al. (1996) considers wind speed, longwave radiation, heat flux, and solar radiation (Fairall96, hereafter). Fairall96 has been included in the COARE 3.5 model (Edson et al., 2013) and recent studies (Alappattu et al., 2017; Embury et al., 2012; Zhang et al., 2020) suggest that Fairall96 better accounts for the cool skin effect than the parameterization dependent upon a single variable (wind speed).

We employ the ERA5 wind speed data (Hersbach et al., 2020) to estimate the Donlon02 cool skin effect. The COARE 3.5 model is used to estimate the Fairall96 cool skin effect. The following model inputs are used: CCI SST v2.1 (European Space Agency Climate Change Initiative SST product;Merchant et al., 2019; Merchant & Embury, 2020), NCEP sea level pressure (Kalnay et al., 1996), ERA5 monthly averaged reanalysis datasets (Hersbach et al.,

2020) for wind speed, 2 m above mean sea level (AMSL) air temperature, relative humidity (calculated from 2 m AMSL air temperature and dewpoint temperature using the August-Roche-Magnus approximation), downward shortwave radiation, downward longwave radiation, and boundary layer height.

2.4 Global Air-Sea CO_2 Flux Estimates with the Temperature Correction

We use two different methods to account for the bias in the SOCAT SST for the global air-sea CO_2 flux estimates. For the first method, we use the buoy SST as the reference temperature to assess the bias in SOCAT SST (bias_buoy, hereafter). We correct the 1° × 1°, monthly fCO_{2w} in SOCAT v2021 via Equation 2 (i.e., $fCO_{2w\_corrected} = fCO_{2w}\, e^{-0.0423 * \Delta SST}$) by the temperature difference (ΔSST) between SOCAT SST and buoy SST. The ΔSST varies with latitude (with a 10° latitude running mean, see the orange line in Figure 2b) but does not vary over time. The number of matched data points between SOCAT SST and buoy SST is small in most years, so ΔSST is averaged over 1982 to 2020. In addition, only fCO_{2w} data within 70°S to 70°N are corrected because of the small number of measurements in the polar oceans. For the second method, the co-located DOISST v2.1 replaces SOCAT SST in Equation 2 to reanalyze fCO_{2w} (bias_OI, hereafter; Watson et al., 2020). The reanalyzed fCO_{2w} is used for the flux calculation (see Goddijn-Murphy et al., 2015 and Holding et al., 2019 for the reanalysis process).

We employ the MPI-SOMFFN neural network technique (Landschützer et al., 2013) to interpolate the $fCO_{2w\_corrected}$ and the reanalyzed fCO_{2w} to the global ocean from 1982 through 2020, using a set of input variables. We use the same datasets as Landschützer et al. (2014) for the neural network inputs, except for the SST product. The CCI SST (Merchant et al., 2019) represents the subskin temperature and is independent of *in-situ* SST measurements, so we utilize the 1° × 1°, monthly CCI SST v2.1 for the neural network training process. The CCI SST v2.1 is also used to calculate Sc and α_w, while the CCI SST v2.1 with a cool skin correction is employed to calculate α_i and fCO_{2a}.

We use two models (Fairall96 and Donlon02) to estimate the cool skin effect. Both Fairall96 and Donlon02 cool skin effect estimates are applied to the CCI SST v2.1 to calculate α_i and fCO_{2a}, respectively. The quadratic wind speed-dependent formulation ($K_{660} = a\, U_{10}^2$; Ho et al., 2006; Wanninkhof, 2014) is used to calculate gas transfer velocity. The 1° × 1°, monthly ERA5 wind speed data from 1982 to 2020 is utilized to scale the transfer coefficient a to match to a global mean K_{660} of 18.2 cm h^{-1} from the ^{14}C inventory method (Naegler, 2009). It is worth noting that the cool skin effect and the warm layer effect do not impact the global mean K_{660} calculated from the ^{14}C inventory because the air-sea ^{14}C concentration difference ($\Delta^{14}C$) is very large (Naegler, 2009; Sweeney et al., 2007), and the upper ocean temperature gradients only result in a minor change in $\Delta^{14}C$. In the end, we substitute all variables above into Equation 1 to calculate the global air-sea CO_2 flux.

3. Results

3.1 Warm Bias in the *In-situ* SOCAT SST

The temperature assessment using the buoy SST suggests a cold bias in the DOISST v2.1 (0.09 K on average) and a small warm bias (0.02 K on average) in the SOCAT SST, which indicates that while a warm bias exists in the SOCAT SST, using the co-located DOISST would overestimate this bias in SOCAT SST (Figure 2a).

Figure 2b shows the latitudinal variation of the bias in SOCAT SST. The number of grid cells with both SOCAT and buoy data (green bars in Figure. 2b) is small and the standard error for the temperature difference (grey shading) is large in the high latitude oceans. Therefore, we only consider data between 70°S and 70°N. The SOCAT SST minus buoy SST (ΔSST, orange line in Figure 2b) shows apparent variation with latitude. ΔSST is on average positive, but is slightly negative at 35°N and 30°S. In the northern hemisphere, ΔSST is +0.04 K near the equator and increases by +0.1 K to a maximum at 25°N and then decreases to -0.05 K at 35°N. ΔSST also increases from 35°N to a maximum of +0.15 K at 50°N and then decreases further north. The ΔSST pattern in the southern hemisphere roughly mirrors that in the northern hemisphere with a 5° northward shift.

It is worth noting that under-sampling affects these bias assessments for SOCAT SST. If we consider all paired cells with both buoy and SOCAT SST measurements, the warm bias is on average +0.02 K. If we only consider cells with at least ten buoy SST and ten SOCAT SST measurements, the warm bias is on average +0.03 K (Figure S2a in Supporting Information S1). The latitudinal variation of the bias is very similar no matter considering how many measurements are within a cell (Figure S2b in Supporting Information S1).

It is important to consider latitudinal variation when correcting for bias in SOCAT SST. For instance, SOCAT SST has a relatively large warm bias (thus a large bias in the fCO_{2w}) in the

Southern Ocean (south of 35°S, Figure 2b), which coupled with a high K_{660} and a large surface ocean area (Figure 2c) results in a substantial bias in Southern Ocean CO_2 flux estimates. This study uses a latitude-varying temperature bias (i.e., the orange line in Figure 2b) to correct the air-sea CO_2 flux between70°S and 70°N (see Section 2.4).

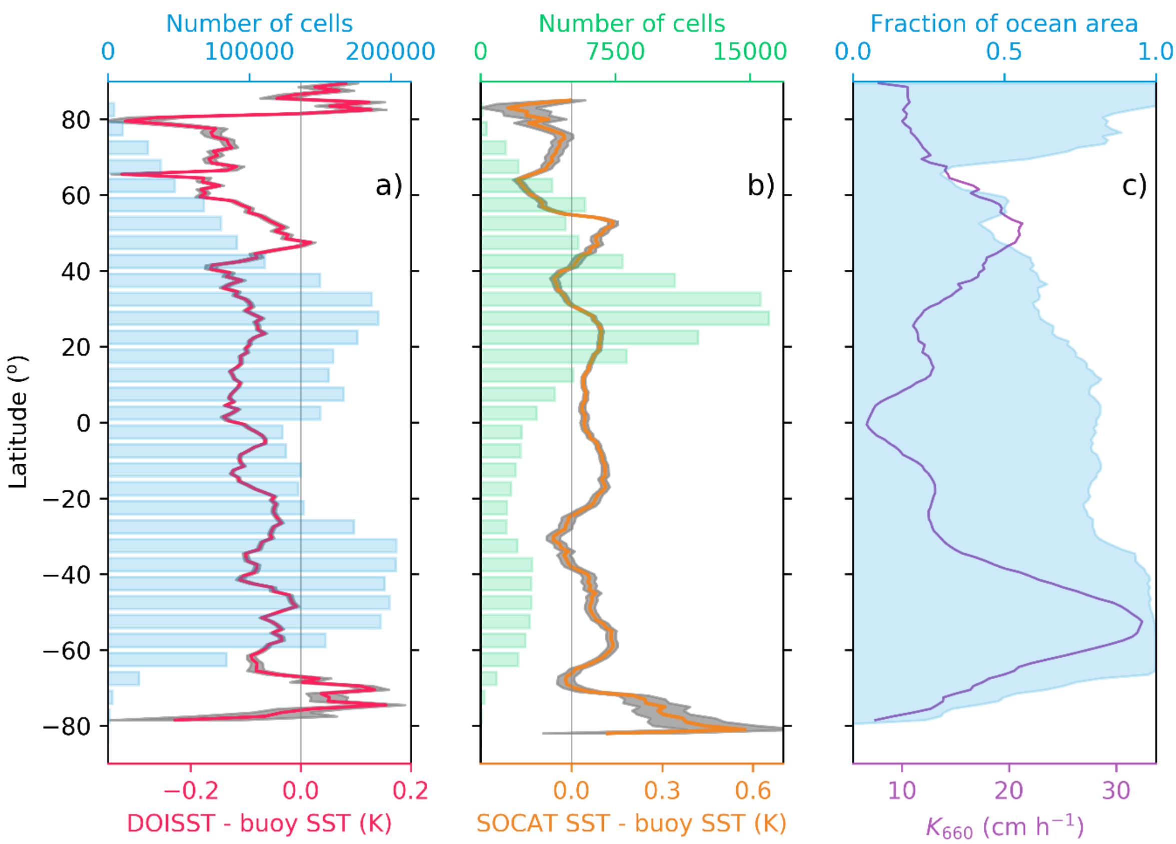

Figure 2. Latitudinal variation in SST differences, number of matched grid cells, the gas transfer velocity (K_{660}) and the fraction of the globe surface area covered by ocean: (a) 1° latitude average temperature difference between DOISST v2.1 and buoy SST (red line) ± 1 standard error (grey shading). The input data are from 1982 to 2020 and have a 1° × 1°, monthly resolution, Blue bars show the number of cells (5° latitude bin) containing both DOISST and buoy SST data; (b) 10° latitude running mean of the temperature difference between SOCAT SST (from SOCATv2021) and buoy SST (orange line, i.e., ΔSST in the main text) ± 1 standard error (grey shading). Green bars correspond to the number of cells (5° latitude bin) containing both gridded SOCAT and buoy SST; (c) 1° latitude average K_{660} (purple line) calculated with a wind speed-dependent parameterization (Ho et al., 2006) using the ERA5 wind speed data (Hersbach et al., 2020) for the global ocean. The blue shaded area corresponds to the fraction of ocean area in different latitudes (1° latitude average).

3.2 The Cool Skin Effect

Figure 3 shows the cool skin effect estimated by Donlon02 and Fairall96. The Fairall96 estimate of the cool skin effect is stronger than the Donlon02 estimate for low wind speeds (U_{10} < 9 m s^{-1}) but weaker for high wind speeds (9 m s^{-1} < U_{10} < 16 m s^{-1}) (Figure 3a). The monthly wind speed distribution (green bars in Figure 3a) shows that wind speeds less than 9 m s^{-1} account for 80% of the wind conditions. Therefore, the cool skin effect estimated by Fairall96 is typically stronger than that estimated by Donlon02. The standard deviation of the Fairall96 cool skin effect is much higher at low wind speeds than at high wind speeds, which reflects that the drivers (longwave radiation, heat flux, and solar radiation) can produce substantial variations in the cool skin effect under relatively calm conditions.

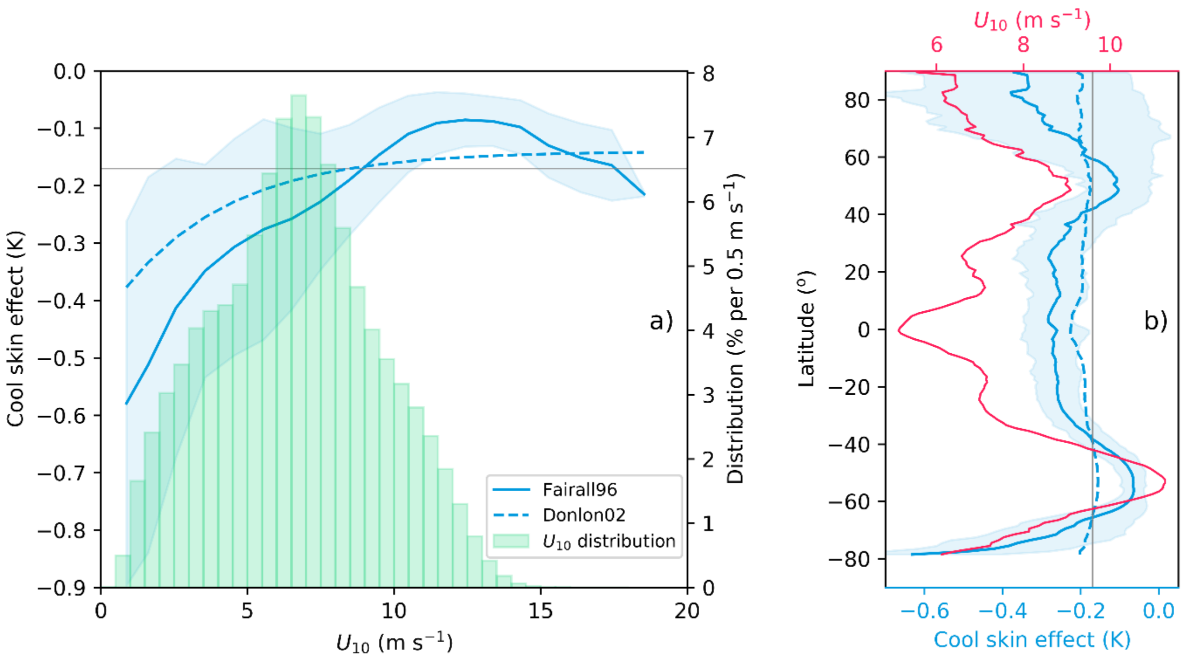

Figure 3. (a) Relationship between the cool skin effect and the 10 m wind speed (U_{10}). Green bars represent the frequency distribution of the ERA5 monthly averaged reanalysis wind speeds (1° × 1°) over the global ocean for 1982–2020. (b) Latitudinal variation in U_{10} (red line) and the cool skin effect (1° latitude bins). Both subplots show the average cool skin effect estimated by the Fairall96 physical model (Fairall et al., 1996, solid blue line), the Donlon02 wind speed-dependent empirical model (Donlon et al., 2002, dashed blue line) and a constant value (-0.17 K, , grey line; Donlon et al., 2002). The light blue shaded area in both subplots indicates one standard deviation of the bin averages in Fairall96 cool skin estimates. Global ocean 1° × 1°, monthly datasets are used to estimate the cool skin effect (see Section 2.3).

The Donlon02 cool skin effect only has a slight latitudinal variation that is not substantially different from a constant (-0.17 K) value (Figure 3b), which was used by a previous study for air-sea CO_2 flux correction (Watson et al., 2020). In contrast, the Fairall96 cool skin estimate shows a clear latitudinal variation with two relatively small cool skin effect regions at around 50°S and 50°N where wind speeds are high. The Fairall96 cool skin effect is stable in the tropical zone and decreases toward both poles to ~50° and then increases at even higher latitudes.

In most ocean regions, the Fairall96 cool skin effect follows variations in wind speed. Intriguingly, the Fairall96 cool skin effect is nearly constant within the tropical and subtropical zones, even though the wind speed is much lower near the equator than in the subtropics. Drivers other than wind speed (i.e., latent and sensible heat fluxes, and longwave radiation) might counteract the low wind speed effect in this area.

4 Discussion

4.1 Variation in the CO_2 Flux Correction

In this section, we discuss the impact of the warm bias and cool skin effects on global air-sea CO_2 flux estimates. The corrections are applied over time (between 1982 and 2020, Figure 4a, b) and by latitude (Figure 4c, d).

The bias correction using the buoy SST assessment (bias_buoy) leads to an average increase in ocean CO_2 uptake of 0.19 Pg C yr^{-1}, while the bias correction utilizing the co-located DOISST (bias_OI) suggests an average increase of 0.43 Pg C yr^{-1} (Figure 4a). Adopting the cool skin correction from Fairall96 and Donlon02 increases the 1982–2020 average ocean CO_2 uptake by 0.39 Pg C yr^{-1} and 0.43 Pg C yr^{-1}, respectively (Figure 4b). A constant cool skin correction of -0.17 K increases the flux by an amount similar to using the Donlon02 correction. In total, the flux correction using the bias_buoy and Fairall96 is on average ~0.3 Pg C yr^{-1} lower than if the bias_OI and Donlon02 are used for 1982 to 2020. The inter-annual variation in the net air-sea CO_2 flux with different temperature corrections are shown in Figure S4 in Supporting Information S1.

Figure 4a and 4c show the change in the air-sea CO_2 flux (ΔFlux) generated by correcting for the warm bias in SOCAT SST. The temporal and the latitudinal variation of the two flux corrections (bias_buoy and bias_OI) follow similar patterns, but the magnitude is different.

Using bias_OI creates a ΔFlux that is twofold larger (in absolute terms) than that using bias_buoy. The data in Figure 2a suggest that using bias_OI may overestimate the bias in SOCAT SST, which would result in a ~0.25 Pg C yr^{-1} overestimation of the air-sea CO_2 flux correction. Therefore, we favour the bias_buoy correction over the bias_OI correction.

While we use the same latitude-varying temperature difference (i.e., bias_buoy) to correct the bias in SOCAT SST for every year, the flux correction shows clear inter-annual variation (green line in Figure 4a). On reason is that the number of measurements in each year of SOCAT is different (Figure S2 in Supporting Information S1), and their spatial distribution differs between years. The latitude-dependent bias correction, when applied to the different year-to-year spatial distribution in the SOCAT data, results in a time-varying annual mean bias correction (Figure S2 in Supporting Information S1).

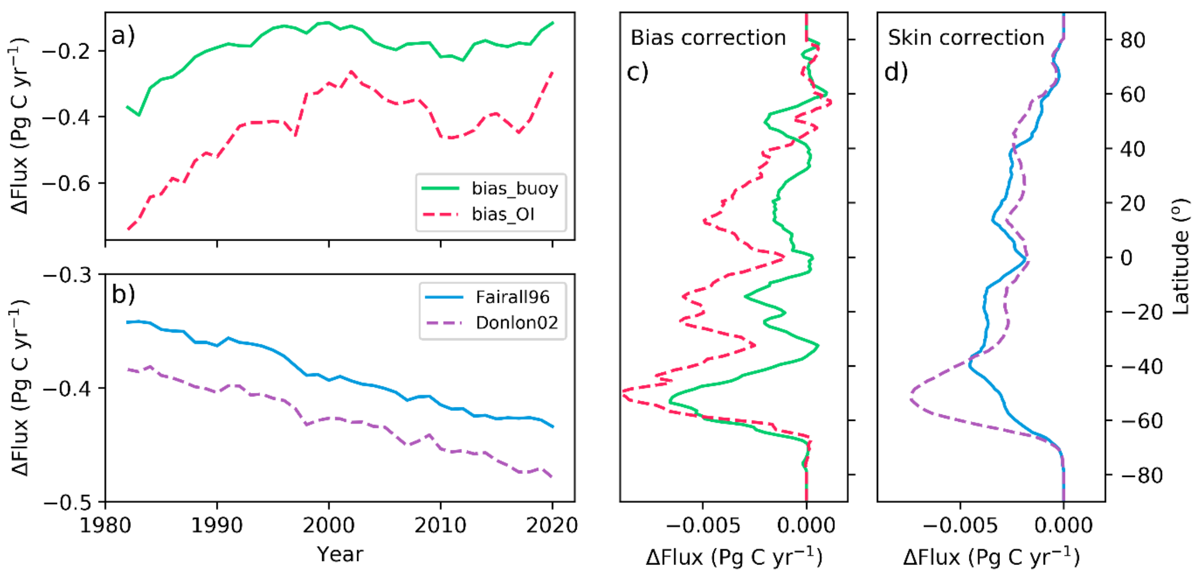

Figure 4. SST corrections to the air-sea CO_2 flux (ΔFlux) versus time (a, b) and versus latitude (c, d). SST corrections account for the bias in the SOCAT SST (a, c) and the cool skin effect (b, d). Negative ΔFlux values represent increased ocean CO_2 uptake. Green and red lines represent ΔFlux due to the bias correction assessed by drifting buoy SST (bias_buoy) and by co-located DOISST (bias_OI), respectively. Blue and purple lines represent ΔFlux due to the Fairall96 and the Donlon02 cool skin corrections, respectively. ΔFlux in a) and b) is the global annual mean, while ΔFlux in (c) and (d) is the long-term average (1982–2020) in 1° latitude bins. Results are based on the MPI-SOMFFN fCO_{2w} mapping method (Landschützer et al., 2013) (See Methods). The inter-annual variation of the global air-sea CO_2 flux with different temperature corrections can be seen in Figure S4 (Supporting Information S1). Our preferred corrections are bias_buoy for warm bias in SOCAT SST and Fairall96 for the cool skin effect (see Section 4.1).

Figure 4b and 4d show the change in air-sea CO_2 flux when accounting for the cool skin effect using the Fairall96 and Donlon02 models. Figure 4b indicates an increase over time in both flux corrections (absolute value), which is driven by the increase in fCO_{2a} (see equation 1 and table 1). The impact of the cool skin effect on the air-sea CO_2 flux is through $\alpha_i * fCO_{2a}$. The ever-rising atmospheric CO_2 concentration and thus fCO_{2a}, result in the growing cool skin flux correction.

The flux correction using Donlon02 exceeds that by Fairall96 by ~0.05 Pg C yr^{-1} (in absolute terms). The largest difference in flux between the two cool skin corrections occurs in the Southern Ocean (Figure 4d). The Donlon02 cool skin effect has minimal latitudinal variation, so the flux correction is largest at ~50°S where the gas transfer velocity is maximum and the ocean area is relatively large (Figure 2c). The Fairall96 cool skin effect has an apparent latitudinal variation and a minimum (absolute) value at ~50°S. This minimum cool skin effect offsets the maximum wind speed and large ocean area, resulting in a smaller flux correction (in absolute terms) at ~50°S for Fairall96 than for Donlon02. Recent work (Alappattu et al., 2017; Embury et al., 2012; Zhang et al., 2020) has suggested that the Fairall96 cool skin model is better than Donlon02 at capturing the cool skin effect at a global scale and this, coupled with our estimates indicates that using the Donlon02 model may lead to an over-correction of the air-sea CO_2 flux, especially in the Southern Ocean.

4.2 Implications for Air-Sea CO_2 Flux Estimates

This study deals with the potential bias in the fCO_{2w}-based air-sea CO_2 flux estimates due to upper ocean temperature effects. A large amount of uncertainty in this fCO_{2w}-based flux also comes from the gas transfer velocity (Woolf et al., 2019). The air-sea CO_2 flux estimated from the ocean carbon inventory (Gruber et al., 2019) does not require the gas transfer velocity, is unaffected by upper ocean temperature effects and provides an independent estimate of ocean CO_2 uptake. To compare the fCO_{2w}-based net air-sea CO_2 flux with the anthropogenic air-sea CO_2 flux of the ocean carbon inventory, we need to adjust for river-induced CO_2 outgassing. The riverine carbon flux has been estimated as 0.23 Pg C yr^{-1} (Lacroix et al., 2020), 0.45 Pg C yr^{-1} (Jacobson et al., 2007), and 0.78 Pg C yr^{-1} (Resplandy et al., 2018). Here we adopt the mean of these values (0.49 ± 0.28 Pg C yr^{-1}).

The net air-sea CO_2 flux derived from the ocean carbon inventory for 1994 to 2007 is -2.1 ± 0.4 Pg C yr^{-1} (i.e., -2.6 Pg C yr^{-1} anthropogenic flux plus 0.49 Pg C yr^{-1} river carbon flux; see the footnote of Table 2 for the propagated uncertainty) (Gruber et al., 2019), which is shown in Table 2 along with the ensemble mean of eighteen fCO_{2w}-based fluxes (Fay et al., 2021). Fluxes from six fCO_{2w} products and three wind speed products (three wind products are used for each fCO_{2w} product) are utilized to generate the ensemble mean flux, where missing fCO_{2w} has been filled with a scaled climatology and gas transfer velocity (K_{660}) has been calibrated to a global average of 18.2 cm hr^{-1} over the ice-free ocean based on ^{14}C-bomb flux estimates (Fay et al., 2021). All six fCO_{2w} products (which include the MPI SOMFFN method) have been developed from the SOCAT v2021 dataset. So the corrections of the ensemble mean flux for the temperature effects should be similar to the corrections in this study based on the MPI-SOMFFN fCO_{2w} mapping method (Landschützer et al., 2013). Futhermore, an ensemble of different data interpolation methods and different wind products provides a more robust flux estimate than a single interpolation method based on a single wind product. The flux corrections estimated in this study are applied to the ensemble mean flux.

Table 2. Global mean net air-sea CO_2 fluxes for 1994 to 2007. Here bias_buoy and bias_OI represent the bias correction (to SOCAT SST) using the assessment from buoy SST and co-located DOISST, respectively. Fairall96 (Fairall et al., 1996) and Donlon02 (Donlon et al., 2002) correspond to the cool skin effect estimated by the physical and the empirical model, respectively. We favour the bias_buoy and Fairall96 corrections (see Section 4.1)

Net air-sea CO_2 flux estimates (Pg C yr^{-1})	**Flux without a temperature correction**	**Flux with warm bias correction**		**Flux with warm bias and cool skin correction**	
		bias_buoy	bias_OI	bias_buoy + Fairall96	bias_OI + Donlon02
Ensemble mean of fCO_{2w}-based fluxes*	-1.7 ± 0.4	-1.8 ± 0.4	-2.0 ± 0.4	-2.2 ± 0.4	-2.4 ± 0.4
Ocean carbon inventory**	-2.1 ± 0.4				

*The ensemble mean of the fluxes from six fCO_2 products and three wind speed products (Fay et al., 2021).

**From Gruber et al. (2019) (-2.6 ± 0.3 Pg C yr^{-1}) with a riverine-derived carbon flux adjustment (0.49 ± 0.28 Pg C yr^{-1}). The uncertainty (i.e., ± 0.4 Pg C yr^{-1}) is calculated as $\sqrt{0.3^2 + 0.28^2}$ Pg C yr^{-1}.

The ensemble mean air-sea CO_2 flux without any bias and cool skin corrections (-1.7 ± 0.4 Pg C yr^{-1}) is barely within the combined uncertainty of the net flux estimate from the ocean carbon inventory. The ensemble mean CO_2 flux with bias_buoy and Fairall96 cool skin corrections is -2.2 ± 0.4 Pg C yr^{-1}, similar to the ocean carbon inventory derived net ocean CO_2 uptake. The corrections using the bias_OI and the Donlon02 suggested by a previous study (Watson et al., 2020) pushes the ensemble mean air-sea CO_2 flux (-2.4 ± 0.4 Pg C yr^{-1}) towards the lower limit of the ocean carbon inventory flux estimate (Table 2).

Another question is whether the warm bias and cool skin flux corrections conflict with our understanding of air-sea CO_2 fluxes. One might argue that the preindustrial ocean and atmosphere would have been in a natural equilibrium (i.e., the global total of steady state of natural air-sea CO_2 fluxes would have been zero; see Hauck et al., 2020 for details), but the temperature corrections would create a preindustrial ocean carbon sink. However, the warm bias in SOCAT SST is not a natural phenomenon and should not affect the preindustrial flux estimate. Furthermore, while the cool skin is a natural phenomenon, the flux correction due to the cool skin effect includes both natural and anthropogenic contributions. Figure 4b shows that the cool skin flux correction decreased almost linearly by ~0.1 Pg C yr^{-1} (from -0.34 to -0.43 Pg C yr^{-1}) due to the increase in atmospheric CO_2 (~70 ppm or μmol mol^{-1}, from 341 to 414 ppm) from 1982 to 2020 (Dlugokencky & Tans, 2018). Preindustrial atmospheric CO_2 was ~260–280 ppm (Wigley, 1983), which is ~70 ppm lower than atmospheric CO_2 in 1982. Thus, the preindustrial natural air-sea CO_2 flux correction due to the cool skin effect could be ~-0.25 Pg C yr^{-1}, with the remaining correction (~-0.2 Pg C yr^{-1} in 2020) due to the increase in atmospheric CO_2 by anthropogenic emissions.

A flux correction for the cool skin effect is only related to the fCO_{2w} observation-based flux estimate, which is available from the 1980s onwards (Friedlingstein et al., 2020). There were no fCO_{2w} measurements in preindustrial times, so the total preindustrial air-sea CO_2 flux (the sum of steady state natural flux and river flux) is based on model studies, theory, and lateral transport constraints (Hauck et al., 2020). Although the cool skin effect might result in an ~-0.25 Pg C yr^{-1} flux, we can still assume that ocean and atmosphere were in a natural equilibrium in preindustrial times. Specifically, the cool skin effect has been implicitly included in the preindustrial natural equilibrium assumption. Therefore, this study improves our understanding by suggesting a stronger anthropogenic contribution to the air-sea CO_2 flux, while there is no contradiction between the temperature correction and the preindustrial natural equilibrium assumption.

The cool skin effect and its impact on the air-sea CO_2 flux have been discussed for decades. While the cool skin effect itself has been well observed and modelled, its impact on the air-sea CO_2 flux is mainly based on theoretical arguments. We still lack strong observational evidence to confirm the need to include the cool skin effect on estimates of air-sea CO_2 flux – an important topic we urge the community to demonstrate experimentally. The eddy covariance method (e.g., Dong et al., 2021) provides direct flux measurements, that could be used as a reference CO_2 flux to assess the accuracy of the bulk CO_2 flux. Long-term eddy covariance measurements at a place with very low ΔfCO_2 would be insightful because the relative effect of cool skin on the bulk CO_2 flux is in theory more prominent for regions of low ΔfCO_2. Appropriate laboratory experiments may yield further insight.

In summary, this work updates the temperature corrections to fCO_{2w}-based air-sea CO_2 flux estimates. It shows that there is a slight warm bias in SOCAT SST and a latitude-varying cool skin effect, resulting in ~0.6 Pg C yr^{-1} additional ocean CO_2 uptake for 1982 to 2020. The corrected air-sea CO_2 flux for an ensemble of six gap filled air-sea CO_2 flux products agrees well with the ocean carbon inventory derived net flux. The extreme sensitivity of fCO_{2w} and thus of the air-sea CO_2 flux to the accuracy of SST means that we should be carefully choose the reference temperature to assess any bias in the SOCAT SST. The importance of the Southern Ocean for atmospheric CO_2 uptake, and the strong winds encountered there mean that large scale assessments need a suitable model for the cool skin correction to the air-sea CO_2 flux.

Acknowledgements

We are grateful to H. Zhang (NOAA), C. Merchant (University of Reading), and H. Beggs (Bureau of Meteorology, Australia) for their advice on choosing the appropriate SST product, as well as to J. Kennedy (Met Office Hadley Centre), and S. Zhou (British Antarctic Survey) for suggestions on assessing the bias in the SOCAT SST. We also greatly appreciate the inspirational and helpful discussions with R. Wanninkhof (NOAA) and J. Shutler (University of Exeter). The Surface Ocean CO_2 Atlas (SOCAT) is an international effort, endorsed by the International Ocean Carbon Coordination Project (IOCCP), the Surface Ocean Lower Atmosphere Study (SOLAS) and the Integrated Marine Biogeochemistry and Ecosystem Research program (IMBER), to deliver a uniformly quality-controlled surface ocean CO_2 database. The many researchers and funding agencies responsible for the collection of data and quality control are thanked for their contributions to SOCAT. In this study,

Y. Dong has been supported by the China Scholarship Council (CSC/201906330072). The Natural Environment Research Council (NERC) has enabled D. C. E. Bakker's work (PICCOLO, NE/P021395/1, and CUSTARD, NE/P021263/1 projects).The contributions of T.G. Bell and M. Yang have been made possible by support from the NERC (ORCHESTRA, NE/N018095/1, and PICCOLO NE/P021409/1 projects) and European Space Agency AMT4oceanSatFluxCCN (4000125730/18/NL/FF/gp).

Open Research

Data can be accessed as follows. Gridded SOCAT v2021 data: https://www.socat.info/index.php/data-access/. Reanalyzed sea surface CO_2 fugacity dataset using co-located DOISST: https://doi.org/10.18160/vmt4-4563. *In-situ* SST measurements (including the drifting buoy SST and the ship SST): https://www.star.nesdis.noaa.gov/socd/sst/iquam/data.html. CCI SST v2.1: https://surftemp.net/regridding/index.html. DOISST v2.1: https://www.ncei.noaa.gov/data/sea-surface-temperature-optimum-interpolation/v2.1/access/avhrr/. ECMWF monthly averaged reanalysis data: https://cds.climate.copernicus.eu/cdsapp#!/dataset/reanalysis-era5-single-levels-monthly-means?tab=form.

References

Alappattu, D. P., Wang, Q., Yamaguchi, R., Lind, R. J., Reynolds, M., & Christman, A. J. (2017). Warm layer and cool skin corrections for bulk water temperature measurements for air-sea interaction studies. *Journal of Geophysical Research: Oceans*, *122*(8), 6470–6481. https://doi.org/10.1002/2017JC012688

Bakker, D. C. E., Alin, S., Castaño-Primo, R., Cronin, M., Gkrizalis, T., Kozyr, A., et al. (2021). SOCAT version 2021 for quantification of ocean CO_2 uptake. Available at https://www.socat.info/index.php/data-access/. Released 15 June 2021.

Bakker, D. C. E., Pfeil, B., Landa, C. S., Metzl, N., O'Brien, K. M., Olsen, A., et al. (2016). A multi-decade record of high-quality fCO_2 data in version 3 of the Surface Ocean CO_2 Atlas (SOCAT). *Earth System Science Data*, *8*(2), 383–413. https://doi.org/10.5194/essd-8-383-2016

Dlugokencky, E., & Tans, P. (2018). Trends in atmospheric carbon dioxide, National Oceanic & Atmospheric Administration, Earth System Research Laboratory (NOAA/ESRL). Available at https://www.socat.info/index.php/data-access/. Last access: 4 February 2022.

Dong, Y., Yang, M., Bakker, D. C. E., Kitidis, V., & Bell, T. G. (2021). Uncertainties in eddy covariance air–sea CO_2 flux measurements and implications for gas transfer velocity parameterisations. *Atmospheric Chemistry and Physics*, *21*(10), 8089–8110. https://doi.org/10.5194/acp-21-8089-2021

Donlon, C. J., Robinson, I., Casey, K. S., Vazquez-Cuervo, J., Armstrong, E., Arino, O., et al. (2007). The global ocean data assimilation experiment high-resolution sea surface temperature pilot project. *Bulletin of the American Meteorological Society*, *88*(8), 1197–1214. https://doi.org/10.1175/BAMS-88-8-1197

Donlon, C. J., Minnett, P. J., Gentemann, C., Nightingale, T. J., Barton, I. J., Ward, B., & Murray, M. J. (2002). Toward improved validation of satellite sea surface skin temperature measurements for climate research. *Journal of Climate*, *15*(4), 353–369. https://doi.org/10.1175/1520-0442(2002)015<0353:TIVOSS>2.0.CO;2

Edson, J. B., Jampana, V., Weller, R. A., Bigorre, S. P., Plueddemann, A. J., Fairall, C. W., et al. (2013). On the exchange of momentum over the open ocean. *Journal of Physical Oceanography*, *43*(8), 1589–1610. https://doi.org/10.1175/JPO-D-12-0173.1

Embury, O., Merchant, C. J., & Corlett, G. K. (2012). A reprocessing for climate of sea surface temperature from the along-track scanning radiometers: Initial validation, accounting for skin and diurnal variability effects. *Remote Sensing of Environment*, *116*, 62–78. https://doi.org/10.1016/j.rse.2011.02.028

Fairall, C. W., Bradley, E. F., Godfrey, J. S., Wick, G. A., Edson, J. B., & Young, G. S. (1996). Cool-skin and warm-layer effects on sea surface temperature. *Journal of Geophysical Research: Oceans*, *101*(C1), 1295–1308. https://doi.org/10.1029/95JC03190

Fay, A. R., Gregor, L., Landschützer, P., McKinley, G. A., Gruber, N., Gehlen, M., et al. (2021). SeaFlux: Harmonization of air-sea CO_2 fluxes from surface pCO_2 data products using a standardized approach. *Earth System Science Data*, *13*(10), 4693–4710. https://doi.org/10.5194/essd-13-4693-2021

Friedlingstein, P., O'Sullivan, M., Jones, M. W., Andrew, R. M., Hauck, J., Olsen, A., et al. (2020). Global carbon budget 2020. *Earth System Science Data*, *12*(4), 3269–3340. https://doi.org/10.5194/essd-12-3269-2020

Gentemann, C. L., & Minnett, P. J. (2008). Radiometric measurements of ocean surface thermal variability. *Journal of Geophysical Research: Oceans*, *113*(C8). https://doi.org/10.1029/2007JC004540

Goddijn-Murphy, L. M., Woolf, D. K., Land, P. E., Shutler, J. D., & Donlon, C. (2015). The OceanFlux Greenhouse Gases methodology for deriving a sea surface climatology of CO_2 fugacity in support of air-sea gas flux studies. *Ocean Science*, *11*(4), 519–541. https://doi.org/10.5194/os-11-519-2015

Gruber, N., Clement, D., Carter, B. R., Feely, R. A., van Heuven, S., Hoppema, M., et al. (2019). The oceanic sink for anthropogenic CO_2 from 1994 to 2007. *Science*, *363*(6432), 1193–1199. https://doi.org/10.1126/science.aau5153

Hauck, J., Zeising, M., Le Quéré, C., Gruber, N., Bakker, D. C. E., Bopp, L., et al. (2020). Consistency and challenges in the ocean carbon sink estimate for the global carbon budget. *Frontiers in Marine Science*, *7*(October), 1–22. https://doi.org/10.3389/fmars.2020.571720

Hersbach, H., Bell, B., Berrisford, P., Hirahara, S., Horányi, A., Muñoz-Sabater, J., et al. (2020). The ERA5 global reanalysis. *Quarterly Journal of the Royal Meteorological Society*, *146*(730), 1999–2049. https://doi.org/10.1002/qj.3803

Ho, D. T., Law, C. S., Smith, M. J., Schlosser, P., Harvey, M., & Hill, P. (2006). Measurements of air-sea gas exchange at high wind speeds in the Southern Ocean: Implications for global parameterizations. *Geophysical Research Letters*, *33*(16). https://doi.org/10.1029/2006GL026817

Holding, T., Ashton, I. G., Shutler, J. D., Land, P. E., Nightingale, P. D., Rees, A. P., et al. (2019). The fluxengine air-sea gas flux toolbox: Simplified interface and extensions for in situ analyses and multiple sparingly soluble gases. *Ocean Science*, *15*(6), 1707–1728. https://doi.org/10.5194/os-15-1707-2019

Huang, B., Liu, C., Banzon, V., Freeman, E., Graham, G., Hankins, B., et al. (2021). Improvements of the daily optimum interpolation sea surface temperature (DOISST) version 2.1. *Journal of Climate*, *34*(8), 2923–2939. https://doi.org/10.1175/JCLI-D-20-0166.1

Jacobson, A. R., Mikaloff Fletcher, S. E., Gruber, N., Sarmiento, J. L., & Gloor, M. (2007). A joint atmosphere-ocean inversion for surface fluxes of carbon dioxide: 1. Methods and global-scale fluxes. *Global Biogeochemical Cycles*, *21*, GB1019. https://doi.org/10.1029/2005GB002556

Jähne, B. (2009). Air-sea gas exchange. *Elements of Physical Oceanography: A Derivative of the Encyclopedia of Ocean Sciences*, 160–169. https://doi.org/10.1016/B978-0-12-409548-9.11613-6

Jähne, B., Heinz, G., & Dietrich, W. (1987). Measurement of the diffusion coefficients of sparingly soluble gases in water. *Journal of Geophysical Research: Oceans*, *92*(C10), 10767–10776. https://doi.org/10.1029/JC092iC10p10767

Johnson, K. S. (1982). Carbon dioxide hydration and dehydration kinetics in seawater. *Limnology and Oceanography*, *27*(5), 849–855. https://doi.org/10.4319/lo.1982.27.5.0849

Kalnay, E., Kanamitsu, M., Kistler, R., Collins, W., Deaven, D., Gandin, L., et al. (1996). The NCEP/NCAR 40-year reanalysis project. *Bulletin of the American Meteorological Society*, *77*(3), 437–472. https://doi.org/10.1175/1520-0477(1996)077<0437:TNYRP>2.0.CO;2

Kennedy, J. J., Rayner, N. A., Smith, R. O., Parker, D. E., & Saunby, M. (2011). Reassessing biases and other uncertainties in sea surface temperature observations measured in situ since 1850: 2. Biases and homogenization. *Journal of Geophysical Research*, *116*(D14), 1–22. https://doi.org/10.1029/2010jd015220

Kennedy, J. J., Rayner, N. A., Atkinson, C. P., & Killick, R. E. (2019). An ensemble data set of sea surface temperature change from 1850: The Met Office Hadley Centre HadSST.4.0.0.0 data set. *Journal of Geophysical Research: Atmospheres*, *124*(14), 7719–7763. https://doi.org/10.1029/2018JD029867

Kent, E. C., Kennedy, J. J., Smith, T. M., Hirahara, S., Huang, B., Kaplan, A., et al. (2017). A call for new approaches to quantifying biases in observations of sea surface temperature. *Bulletin of the American Meteorological Society*, *98*(8), 1601–1616. https://doi.org/10.1175/BAMS-D-15-00251.1

Lacroix, F., Ilyina, T., & Hartmann, J. (2020). Oceanic CO_2 outgassing and biological production hotspots induced by pre-industrial river loads of nutrients and carbon in a global modeling approach. *Biogeosciences*, *17*(1), 55–88. https://doi.org/10.5194/bg-17-55-2020

Landschützer, P., Gruber, N., Bakker, D. C. E., Schuster, U., Nakaoka, S., Payne, M. R., et al. (2013). A neural network-based estimate of the seasonal to inter-annual variability of the Atlantic Ocean carbon sink. *Biogeosciences*, *10*(11), 7793–7815. https://doi.org/10.5194/bg-10-7793-2013

Landschützer, P., Gruber, N., & Bakker, D. C. E. (2020). An observation-based global monthly gridded sea surface pCO_2 and air-sea CO2 flux product from 1982 onward and its monthly climatology. *NCEI Accession*, *160558*.

Landschützer, P., Gruber, N., Bakker, D. C. E., & Schuster, U. (2014). Recent variability of the global ocean carbon sink. *Global Biogeochemical Cycles*, *28*(9), 927–949. https://doi.org/10.1002/2014GB004853

Liss, P. S., & Slater, P. G. (1974). Flux of gases across the air-sea interface. *Nature*, *247*(5438), 181–184. https://doi.org/10.1038/247181a0

Merchant, C. J., & Embury, O. (2020). Adjusting for desert-dust-related biases in a climate data record of sea surface temperature. *Remote Sensing*, *12*(16), 1–15. https://doi.org/10.3390/RS12162554

Merchant, C. J., Embury, O., Bulgin, C. E., Block, T., Corlett, G. K., Fiedler, E., et al. (2019). Satellite-based time-series of sea-surface temperature since 1981 for climate applications. *Scientific Data*, *6*(1), 1–18. https://doi.org/10.1038/s41597-019-0236-x

Minnett, P. J., Smith, M., & Ward, B. (2011). Measurements of the oceanic thermal skin effect. *Deep-Sea Research Part II: Topical Studies in Oceanography*, *58*(6), 861–868. https://doi.org/10.1016/j.dsr2.2010.10.024

Naegler, T. (2009). Reconciliation of excess ^{14}C-constrained global CO_2 piston velocity estimates. *Tellus, Series B: Chemical and Physical Meteorology*, *61* (2), 372–384. https://doi.org/10.1111/j.1600-0889.2008.00408.x

Nightingale, P. D., Malin, G., Law, C. S., Watson, A. J., Liss, P. S., Liddicoat, M. I., et al. (2000). In situ evaluation of air-sea gas exchange parameterizations using novel conservative and volatile tracers. *Global Biogeochemical Cycles*, 14(1), 373–387. https://doi.org/10.1029/1999GB900091

O'Carroll, A. G., Armstrong, E. M., Beggs, H., Bouali, M., Casey, K. S., Corlett, G. K., et al. (2019). Observational needs of sea surface temperature. *Frontiers in Marine Science*, *7*:571720. https://doi.org/10.3389/fmars.2019.00420

Pfeil, B., Olsen, A., Bakker, D. C. E., Hankin, S., Koyuk, H., Kozyr, A., et al. (2013). A uniform, quality controlled Surface Ocean CO_2 Atlas (SOCAT). *Earth System Science Data*, *5*(1), 125–143. https://doi.org/10.5194/essd-5-125-2013

Prytherch, J., Farrar, J. T., & Weller, R. A. (2013). Moored surface buoy observations of the diurnal warm layer. *Journal of Geophysical Research: Oceans*, *118*(9), 4553–4569. https://doi.org/10.1002/jgrc.20360

Resplandy, L., Keeling, R. F., Rödenbeck, C., Stephens, B. B., Khatiwala, S., Rodgers, K. B., et al. (2018). Revision of global carbon fluxes based on a reassessment of oceanic and riverine carbon transport. *Nature Geoscience*, *11*(7), 504–509. https://doi.org/10.1038/s41561-018-0151-3

Reynolds, R. W., & Chelton, D. B. (2010). Comparisons of daily sea surface temperature analyses for 2007-08. *Journal of Climate*, *23*(13), 3545–3562. https://doi.org/10.1175/2010JCLI3294.1

Reynolds, R. W., Smith, T. M., Liu, C., Chelton, D. B., Casey, K. S., & Schlax, M. G. (2007). Daily high-resolution-blended analyses for sea surface temperature. *Journal of Climate*, *20*(22), 5473–5496. https://doi.org/10.1175/2007JCLI1824.1

Robertson, J. E., & Watson, A. J. (1992). Thermal skin effect of the surface ocean and its implications for CO_2 uptake. *Nature*, *358*(6389), 738–740. https://doi.org/10.1038/358738a0

Sabine, C. L., Feely, R. A., Gruber, N., Key, R. M., Lee, K., Bullister, J. L., et al. (2004). The oceanic sink for anthropogenic CO_2. *Science*, *305*(5682), 367–371.

https://doi.org/10.1126/science.1097403

Sabine, C. L., Hankin, S., Koyuk, H., Bakker, D. C. E., Pfeil, B., Olsen, A., et al. (2013). Surface Ocean CO_2 Atlas (SOCAT) gridded data products. *Earth System Science Data*, *5*(1), 145–153. https://doi.org/10.5194/essd-5-145-2013

Saunders, P. M. (1967). The temperature at the ocean-air interface. *Journal of Atmospheric Sciences*, *24*(3), 269–273. https://doi.org/10.1175/1520-0469(1967)024<0269:TTATOA>2.0.CO;2

Shutler, J. D., Wanninkhof, R., Nightingale, P. D., Woolf, D. K., Bakker, D. C. E., Watson, A., et al. (2019). Satellites will address critical science priorities for quantifying ocean carbon. *Frontiers in Ecology and the Environment*, *18*(1): 27– 35. https://doi.org/10.1002/fee.2129

Sweeney, C., Gloor, E., Jacobson, A. R., Key, R. M., McKinley, G., Sarmiento, J. L., & Wanninkhof, R. (2007). Constraining global air-sea gas exchange for CO_2 with recent bomb ^{14}C measurements. *Global Biogeochemical Cycles*, *21*, GB2015. https://doi.org/10.1029/2006GB002784

Takahashi, T., Olafsson, J., Goddard, J. G., Chipman, D. W., & Sutherland, S. C. (1993). Seasonal variation of CO_2 and nutrients in the high-latitude surface oceans: A comparative study. *Global Biogeochemical Cycles*, *7*(4), 843–878. https://doi.org/10.1029/93GB02263

Takahashi, T., Sutherland, S. C., Wanninkhof, R., Sweeney, C., Feely, R. A., Chipman, D. W., et al. (2009). Climatological mean and decadal change in surface ocean pCO_2, and net sea-air CO_2 flux over the global oceans. *Deep Sea Research Part II: Topical Studies in Oceanography*, *56*(8–10), 554–577. https://doi.org/10.1016/J.DSR2.2008.12.009

Wanninkhof, R. (2014). Relationship between wind speed and gas exchange over the ocean revisited. *Limnology and Oceanography: Methods*, *12*, 351–362. https://doi.org/10.4319/lom.2014.12.351

Wanninkhof, R., Asher, W. E., Ho, D. T., Sweeney, C., & McGillis, W. R. (2009). Advances in quantifying air-sea gas exchange and environmental forcing. *Annual Review of Marine Science*, *1*(1), 213–244. https://doi.org/10.1146/annurev.marine.010908.163742

Ward, B., Wanninkhof, R., McGillis, W. R., Jessup, A. T., DeGrandpre, M. D., Hare, J. E., & Edson, J. B. (2004). Biases in the air-sea flux of CO_2 resulting from ocean surface temperature gradients. *Journal of Geophysical Research C: Oceans*, *109*(8), 1–14. https://doi.org/10.1029/2003JC001800

Watson, A. J., Schuster, U., Shutler, J. D., Holding, T., Ashton, I. G. C., Landschützer, P., et al. (2020). Revised estimates of ocean-atmosphere CO_2 flux are consistent with ocean carbon inventory. *Nature Communications*, *11*(1), 1–6. https://doi.org/10.1038/s41467-020-18203-3

Weiss, R. F. (1974). Carbon dioxide in water and seawater: the solubility of a non-ideal gas. *Marine*

Chemistry, *2*(3), 203–215. https://doi.org/10.1016/0304-4203(74)90015-2

Wigley, T. M. L. (1983). The pre-industrial carbon dioxide level. *Climatic Change*, *5*(4), 315–320. https://doi.org/10.1007/BF02423528

Woolf, D. K., Land, P. E., Shutler, J. D., Goddijn-Murphy, L. M., & Donlon, C. J. (2016). On the calculation of air-sea fluxes of CO_2 in the presence of temperature and salinity gradients. *Journal of Geophysical Research: Oceans*, *121*(2), 1229–1248. https://doi.org/10.1002/2015JC011427

Woolf, D. K., Shutler, J. D., Goddijn-Murphy, L., Watson, A. J., Chapron, B., Nightingale, P. D., et al. (2019). Key uncertainties in the recent air-sea flux of CO_2. *Global Biogeochemical Cycles*, *33*(12), 1548–1563. https://doi.org/10.1029/2018GB006041

Xu, F., & Ignatov, A. (2014). In situ SST quality monitor (*i*Quam). *Journal of Atmospheric and Oceanic Technology*, *31*(1), 164–180. https://doi.org/10.1175/JTECH-D-13-00121.1

Yang, C., Leonelli, F. E., Marullo, S., Artale, V., Beggs, H., Nardelli, B. B., et al. (2021). Sea surface temperature intercomparison in the framework of the copernicus climate change service (C3S). *Journal of Climate*, *34*(13), 5257–5283. https://doi.org/10.1175/JCLI-D-20-0793.1

Zeebe, R. E., & Wolf-Gladrow, D. (2001). *CO_2 in seawater: equilibrium, kinetics, isotopes*. Elsevier Science, pp. 85–140.

Zhang, H., Beggs, H., Ignatov, A., & Babanin, A. V. (2020). Nighttime cool skin effect observed from infrared SST autonomous radiometer (ISAR) and depth temperatures. *Journal of Atmospheric and Oceanic Technology*, *37*(1), 33–46. https://doi.org/10.1175/JTECH-D-19-0161.1

AGU PUBLICATIONS

Global Biogeochemical Cycles

Supporting Information for

Update on the Temperature Corrections of Global Air-Sea CO_2 Flux Estimates

Yuanxu Dong[1,2], Dorothee C. E. Bakker[1]*, Thomas G. Bell[2], Boyin Huang[3], Peter Landschützer[4], Peter S. Liss[1], Mingxi Yang[2]

[1]Centre for Ocean and Atmospheric Sciences, School of Environmental Sciences, University of East Anglia, Norwich, UK; [2]Plymouth Marine Laboratory, Prospect Place, Plymouth, UK; [3]National Centers for Environmental Information, National Oceanic and Atmospheric Administration, Asheville, NC, USA; [4]Max Planck Institute for Meteorology, Hamburg, Germany

Correspondence to: Yuanxu Dong (Yuanxu.Dong@uea.ac.uk) and Dorothee C. E. Bakker (D.Bakker@uea.ac.uk)

Contents of this file

Additional Supporting Information (Files uploaded separately)

Dataset S1

Text S1. Conversion of CO_2 Concentration

The mole fraction of the equilibrated CO_2 (χCO_{2w}) in the equilibrator is measured by a gas analyzer and is then converted into CO_2 partial pressure (pCO_{2w_equ}) using the equilibrator temperature (T_{equ}, K) and pressure (P_{equ}, atm):

$$pCO_{2w\_equ} = \chi CO_{2w}(P_{equ} - pH_2O) \quad \text{(S1)}$$

where pH_2O (atm) is the water vapor pressure and can be calculated from T_{equ} and the seawater salinity (Pierrot et al., 2009). The pCO_{2w_equ} is then converted into fCO_{2w_equ} to correct for non-ideal behavior of the gas (Weiss, 1974):

$$fCO_{2w\_equ} = \gamma \, pCO_{2w\_equ} \quad \text{(S2)}$$

where the fugacity coefficient γ is ~0.996 (Bakker et al., 2014).

Text S2. The Timescale of Chemical Repartitioning and Water Mass Transport

The seawater carbonate system creates unique properties for air-sea CO_2 exchange. The seawater carbonate system includes several different carbonate species, i.e., CO_2, carbonic acid, bicarbonate, carbonate. Among these species, only CO_2 is directly involved in the air-sea CO_2 exchange. There is a dynamic equilibrium between these carbonate species. When the seawater temperature varies, these carbonate species repartition and gradually approach a new equilibrium. The relaxation time (the time after which a perturbation has reached e^{-1} of its initial value) for this equilibration depends on pH and temperature. For typical seawater (pH ~8.2, total dissolved inorganic carbon ~2000 μmol kg^{-1}, and salinity ~35) at ~25°C, the relaxation time is ~13 s (Johnson, 1982; Zeebe & Wolf-Gladrow, 2001). For warmer seawater (e.g., ~30°C), the relaxation time is shorter (~11 s) (Johnson, 1982; Zeebe & Wolf-Gladrow, 2001), while for colder seawater, the relaxation time is longer. Therefore, the timescale of the chemical repartitioning of the CO_2 system is at least 10 s. i.e., if the seawater temperature varies, more than 10 s is required for the carbonate species to approach equilibrium.

There is a temperature gradient in the thermal boundary layer (TBL), and the temperature at the top of the TBL is lower than that at the bottom of the TBL due to the cool skin effect. The typical thickness of the TBL (L) is 1 mm (Jähne, 2009). The mass boundary layer (MBL) is at the top of the TBL with a typical thickness of 0.1 mm (Jähne, 2009). Molecular diffusion dominates water mass transport within MBL. There is a viscous boundary layer (VBL) below the MBL and the VBL has a similar thickness as the TBL (i.e., L ~1 mm) (Jähne, 2009). Viscous dissipation dominates water mass transport in the VBL (Jähne, 2009). The kinematic viscosity (v) is ~1 $mm^2\ s^{-1}$ at 25°C seawater (v is larger at colder seawater). So, the timescale of water mixing in the TBL (below the MBL) is ~1 s (L^2/v).

Text S3. SST Dataset for Air-Sea CO_2 Flux Estimates

The SST data used for flux estimates differ between studies. Table S1 lists SST datasets used in eight global observation-based (i.e., fCO_2-based) air-sea CO_2 flux estimates. Within a specific study, the same global gap-free SST dataset is typically used for the calculation of Schmidt number, *Sc*, solubility at the base of the MBL, α_w, and at the air-sea interface, α_i, CO_2 fugacity in the atmosphere, fCO_{2a}, and for the fCO_{2w} mapping, while the *in-situ* bulk water temperature (T_{Bulk}) measured concurrently with fCO_{2w} is used for correcting individual fCO_{2w} from the equilibrator temperature to the seawater temperature.

An exception to the above is Watson et al. (2020), which co-located the DOISST v2.0 ($1° \times 1°$, monthly data) (Reynolds et al., 2007) to the individual fCO_{2w} measurements in SOCAT (Goddijn-Murphy et al., 2015). The co-located DOISST v2.0 was used to re-calculate fCO_{2w} (via Equation 2 in the main text). Watson et al. (2020) showed that SOCAT SST is on average 0.13 ± 0.78 K higher than the co-located DOISST v2.0, and the SOCAT fCO_{2w} is on average 1.65 ± 11.98 µatm higher than the re-calculated fCO_{2w}. Watson et al. (2020) and this study are the only two studies that considered the cool skin effect. Watson et al. (2020) applied a constant cool skin correction (0.17 K) to the satellite subskin SST product (i.e., DOISST v2.0 minus 0.17 K) for the calculation of α_i and fCO_{2a}. In addition, Watson et al. (2020) used HadISST for the mapping process instead of the SST product used to calculate the other variables (i.e., DOISST v2.0).

As discussed in the main text, a global gap-free $T_{Subskin}$ product is an important practical SST for the air-sea CO_2 flux calculation. However, only some of the global gap-free SST products in Table S1 (MOISST v2, DOISST v2.0, OAFlux, and CCI SST v2.1) represent the subskin temperature, while the others (ASMD, ARMOR3D, MGDSST, HadISST) correspond to the temperature of bulk seawater.

Text S4. Comparison of Three Satellite SST Products

The satellite SST product is expected to provide a consistent subskin temperature which can be used for calculating global *Sc*, α_w, α_i, and fCO_{2a}, and for mapping fCO_{2w}. Recent research compared eight global gap-free satellite/blend SST products (ESA CCI SST v2.0, ERA5, HadISST1, DOISST v2.1, MUR25 v4.2, MGDSST, BoM Monthly SST, OSITASST) and showed that the global mean of these eight SST products ranges from 20.02 °C to 20.17 °C (for the period 2003-2018 with 95% confidence level) (Yang et al., 2021). So, a bias potentially exists in some or all of these satellite SST products. In addition, among these eight satellite SST products, only the CCI SST (Merchant et al., 2019; Merchant & Embury, 2020) and the DOISST (Huang et al., 2021; Reynolds et al., 2007) represent the subskin temperature (Yang et al., 2021). The other SST products provide a bulk temperature for a depth below the subskin. So, hereafter, only the CCI SST and the OISST (DOISST and MOISST) are assessed.

There are two types of OISST products: 1) 1° × 1°, monthly OI.V2 SST (MOISST), which is derived by linear interpolation of the 1° × 1°, weekly OI.v2 SST fields to daily fields which are then averaged over a month (Reynolds et al., 2002); 2) 1/4° × 1/4°, daily OISST v2 (Reynolds et al., 2007) which has been replaced by DOISST v2.1 (Huang et al., 2021) with some quality improvements for data from January 1, 2016, onwards. DOISST data are constructed differently than the MOISST, although both use satellite-derived SST data with a calibration based on *in-situ* measurements (including both ICOADS ship and drifting buoy SST) (Freeman et al., 2017; Xu & Ignatov, 2014). With the warm bias in the ICOADS ship SST well-recognized by the SST community (Huang et al., 2017; Kennedy et al., 2011, 2019), a constant (0.14 K) is subtracted from the ICOADS ship SST to compensate for the large scale (global mean) ship-buoy SST difference (Reynolds & Chelton, 2010) before it is used to calibrate the DOISST v2.0. In addition, the latest research shows that the bias in the ICOADS ship SST has substantially reduced since 2006 (Kennedy et al., 2019). So for the DOISST v2.1 dataset, the ship-buoy SST difference has been set to 0.14 K from 1981 to 2015 and to 0.01 K from 2016 onwards (Huang et al., 2021). However, the warm bias in the ICOADS ship SST is not corrected for when it is used for the calibration of the MOISST. So the DOISST tends to be lower than the monthly MOISST, particularly in the 1980s and 1990s when ship SST data were dominant (Banzon et al., 2016).

Here we test the agreement between the gridded drifting buoy SST (as a reference SST; Xu & Ignatov, 2014) and three satellite SST products: CCI SST v2.1, MOISST v2, DOISST v2.1. Figure S1a shows a comparison between different SST products. The DOISST v2.1 is on average 0.09 K lower than the buoy SST (red curve), while the MOISST v2 is on average 0.01 K lower than the buoy SST (blue curve). The orange curve shows that the CCI SST v2.1 is on average 0.05 K lower than the buoy SST.

Although MOISST v2 has the smallest bias, it is an old SST product and has not been updated for a long time. The standard deviation (SD) of MOISST minus the buoy SST (blue line in Figure S1b) is larger than that of DOISST v2.1 (or CCI SST v2.1) minus buoy SST (red and orange lines in Figure S1b). Therefore, we suggest that the MOISST should better not be used for air-sea CO_2 flux estimates.

The SD of DOISST v2.1 minus the buoy SST is similar to the SD of CCI SST v2.1 minus the buoy SST (red and orange line in Figure S1b). Therefore, both DOISST v2.1 and CCI SST v2.1 can be used for the air-sea CO_2 flux estimates (i.e., calculating global Sc, α_w, α_i, fCO_{2a}, and mapping fCO_{2w}). However, as the *in-situ* SST measurements were employed for the validation process, DOISST and MOISST are not fully independent from the *in-situ* SSTs. The CCI SST is independent from the *in-situ* SST dataset because the CCI SST is not calibrated against *in-situ* SST measurements as a reduced-state-vector optimal estimation algorithm (Merchant et al., 2019) is used instead.

The purple line in Figure S1b shows that the SD of CCI SST v2.1 minus DOISST v2.1 is ~0.5 K and decreasing to ~0.4 K in recent years, which suggests that there is a discrepancy between these two satellite SST products. the SD of DOISST v2.0 minus SOCAT SST is ~0.8 K. The large SDs suggest that using any co-located satellite SST products to calculate fCO_{2w} could significantly increase the uncertainty in fCO_{2w} and thus the uncertainty in the estimated air-sea CO_2 flux.

Text S5. Under-Sampling and inter-Annual Variation of the Bias Correction

Due to the limited measurements in SOCAT and buoy SST datasets, especially during the 1980s, many grid cells only have a small number of SOCAT and buoy SST measurements. The number of measurements in grid cells might influence the comparison between the SOCAT SST and the buoy SST. Figure S2a shows the under-sampling issue and its influence on the average of SOCAT SST minus buoy SST. If we consider all matched grid cells, the average of SOCAT SST minus buoy SST is ~0.02 K. But if we consider cells with at least 10 measurements, the average of SOCAT SST minus buoy SST is ~0.03 K. However, Figure S2b suggests that under-sampling does not significantly influence the latitudinal variation of SOCAT SST minus buoy SST.

Figure S3 shows the inter-annual variation of the number of cells with SOCAT measurements and the bias correction for the SOCAT SST. We apply the latitudinal-varying bias correction (red curve in Figure S2b) to account for the bias in the SOCAT SST (use buoy SST as the reference). However, as the number of SOCAT measurements varies with year, and the measurements in years before 1990 are limited (blue bars in Figure S3), we do not consider inter-annual variation of the latitudinal-varying bias correction. Thus, the same bias correction value is applied to a specific latitude for every year (every month) between 1982 and 2020. However, as the spatial distribution of the SOCAT measurements is different in different years, the annual mean bias correction varies with year (red line in Figure S3).

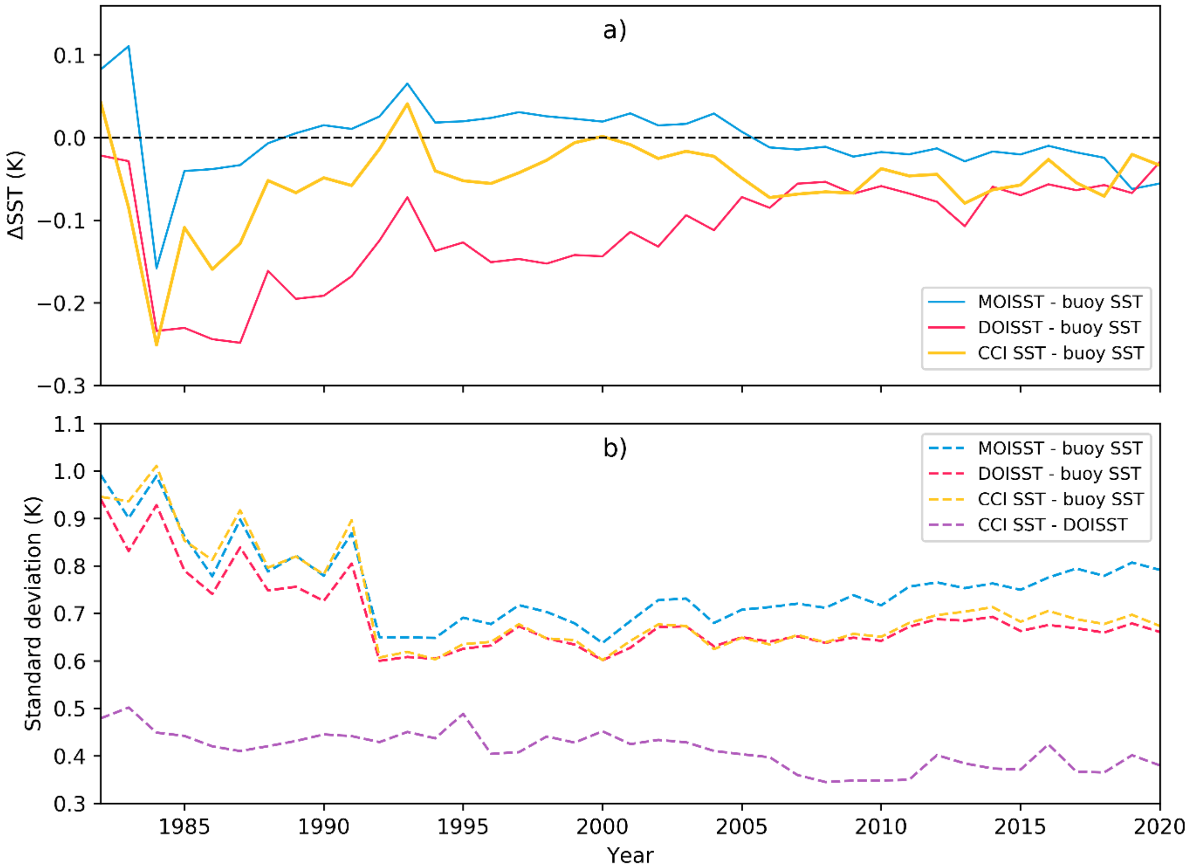

Figure S1. Time series of the global annual mean SST difference and its standard deviation between SST products. (a) The blue, red and orange lines represent the MOISST v2 (MOISST) minus drifting buoy SST, DOISST v2.1 (DOISST) minus buoy SST, and ESA CCI SST v2.1 (CCI SST) minus buoy SST, respectively. (b) The blue, red, orange, and purple dashed lines correspond to the standard deviation of MOISST minus buoy SST, DOISST minus buoy SST, CCI SST and buoy SST, and CCI SST minus DOISST, respectively.

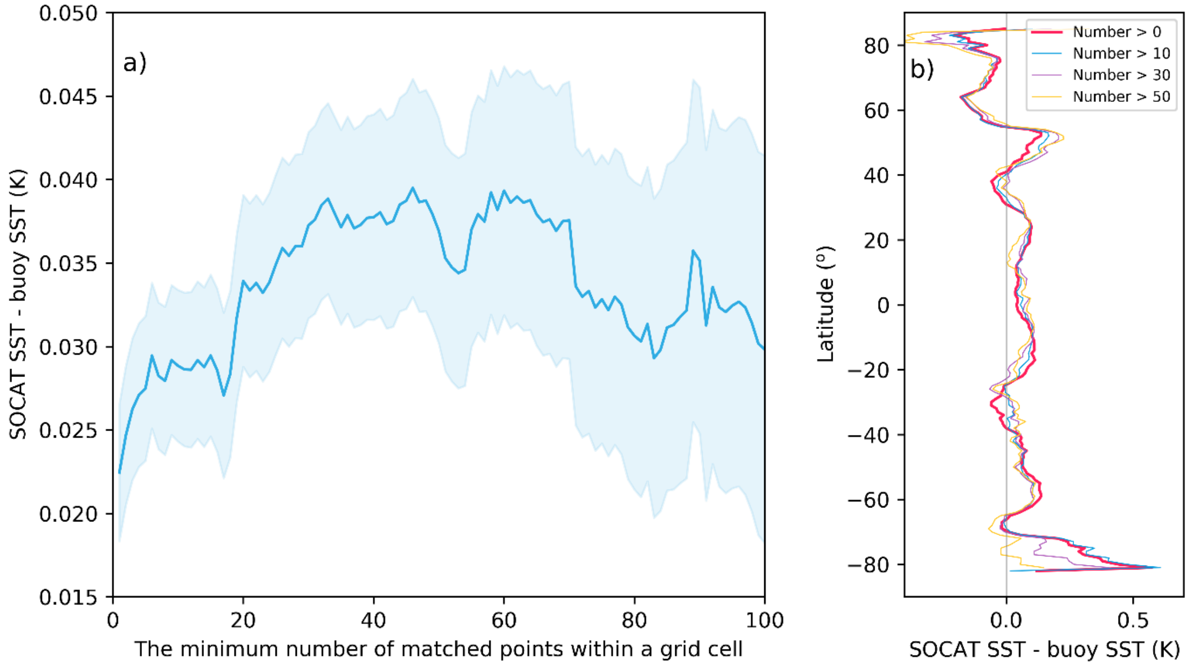

Figure. S2. (a) Average of SOCAT SST minus buoy SST (from 1982 to 2020) versus the minimum number of matched points within a grid cell, and (b) the latitudinal variation of SOCAT SST minus buoy SST. The first (second) point in (a) represents the average temperature difference considering all grid cells with at least one (two) SOCAT and one (two) buoy measurement (s). The blue shading indicates one standard deviation. The red, blue, purple, and orange lines in (b) correspond to the average temperature difference for grid cells with at least one, eleven, thirty one, and fifty one matched SOCAT and buoy measurements, respectively .

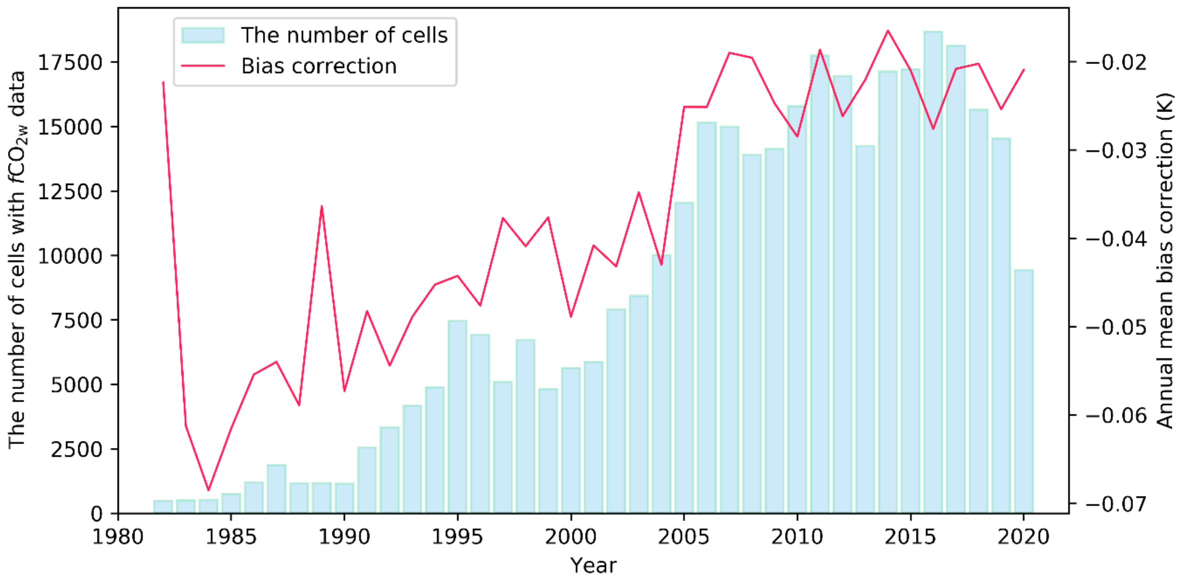

Figure S3. The number of grid cells (per year) with measurements in the 1° × 1°, monthly gridded SOCAT data (blue bars) and the inter-annual mean bias correction for the SOCAT SST (red line) assessed by the buoy SST.

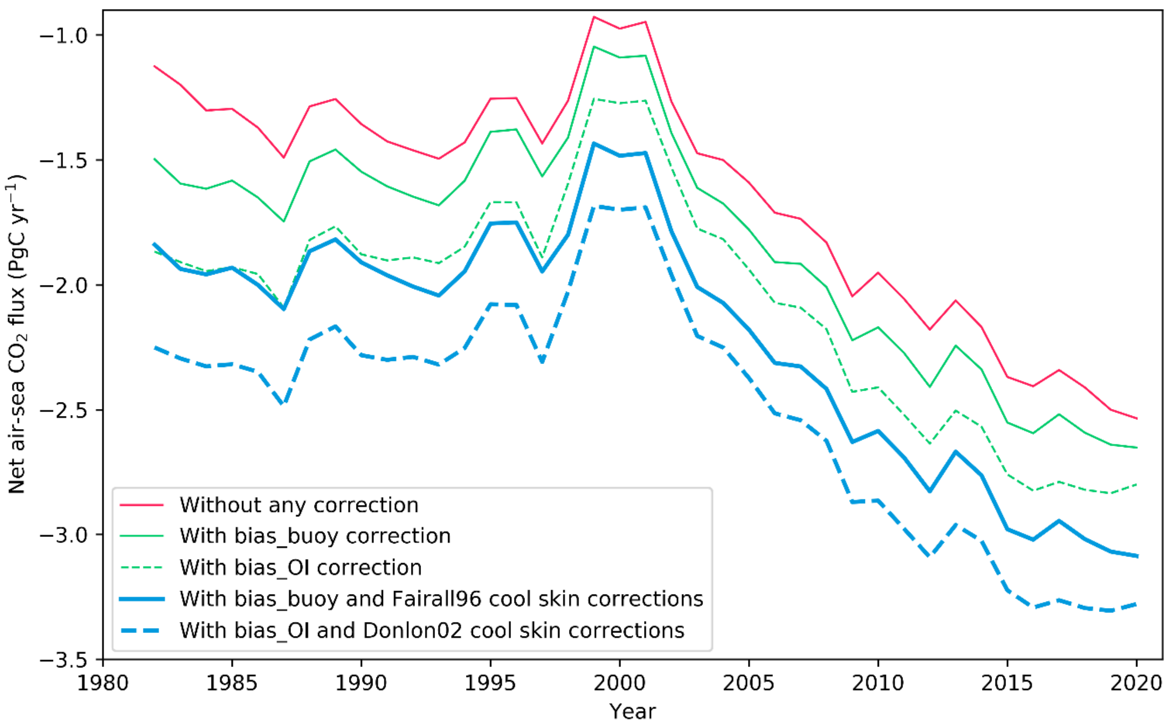

Figure S4. Time series of the annual mean global net air-sea CO_2 flux calculated by interpolating the sea surface CO_2 fugacity (fCO_{2w}) data in SOCATv2021 using a neural network-based method (Landschützer et al., 2013). Negative values represent ocean CO_2 uptake. The red, green, and blue solid lines represent the uncorrected flux, the flux with bias_buoy correction (bias assessed by buoy SST), and the flux with bias_buoy and Fairall96 cool skin corrections, respectively (this study). The green and blue dashed curves correspond to the flux with the bias_OI (using co-located DOISST v2.1 to account for the bias in SOCAT SST) and Donlon02 cool skin corrections (Watson et al., 2020). The same datasets, interpolation method (Landschützer et al., 2013), and the Arctic and the coastal flux compensation method (Fay et al., 2021) are used for the flux calculations in the figure.

Table S1. Summary of the SST datasets used in global air-sea CO_2 flux estimates by the bulk flux method (Equation 1 in the main text). Acronyms of SST products and related references are in the footnotes.

Studies	Sc and α_w	α_i and fCO_{2a}	Individual fCO_{2w}	fCO_{2w} mapping
Takahashi et al. (2009)	ASMD	ASMD	*In-situ* T_{Bulk}	Interpolated T_{Bulk}
Rödenbeck et al. (2013)	OAFlux	OAFlux	*In-situ* T_{Bulk}	OAFlux
Zeng et al. (2014) and Landschützer et al. (2016)	MOISST v2	MOISST v2	*In-situ* T_{Bulk}	MOISST v2
Denvil-Sommer et al. (2019)	ARMOR3D	ARMOR3D	*In-situ* T_{Bulk}	ARMOR3D
Gregor et al. (2019)	DOISST v2.0	DOISST v2.0	*In-situ* T_{Bulk}	DOISST v2.0
Watson et al. (2020)	DOISST v2.0	DOISST v2.0 – 0.17 K	Co-located DOISST v2.0	HadISST
Iida et al. (2021)	MGDSST	MGDSST	*In-situ* T_{Bulk}	MGDSST
This study	CCI SST v2.1	CCI SST v2.1 with a Fairall96 cool skin correction	*In-situ* T_{Bulk} with a bias correction assessed by buoy SST	CCI SST v2.1

ASMD: surface water temperature from the NOAA Atlas of Surface Marine Data (1994, as cited in Takahashi et al., 2009). OAFlux: SST from the Objectively Analysed Air-Sea Fluxes for the global oceans dataset (Yu & Weller, 2007). MOISST v2: NOAA Monthly Optimum Interpolation SST dataset version 2, also known as OI.V2 SST (Reynolds et al., 2002). ARMOR3D: SST from monthly global reprocessed products of physical variables from the ARMOR3D L4 dataset (Guinehut et al., 2012). DOISST v2.0: NOAA Daily Optimum Interpolation SST dataset version 2 (Banzon et al., 2016; Reynolds et al., 2007). HadISST: Hadley Centre Sea Ice and Sea Surface Temperature dataset (Rayner et al., 2003). MGDSST: Merged satellite and *in-situ* data global daily SST analysis dataset (Sakurai et al., 2005). CCI SST v2.1: European Space Agency Climate Change Initiative SST product (Merchant et al., 2019; Merchant & Embury, 2020). *In-situ* T_{Bulk} represents the *in-situ* bulk SST measurements in the LDEO and SOCAT datasets. The study of Takahashi et al. (Takahashi et al., 2009) used the LDEO (Lamont-Doherty Earth Observatory) fCO_{2w} dataset (Takahashi et al., 2008) while the other studies employed the SOCAT fCO_{2w} dataset (Bakker et al., 2016). Co-located DOISST v2.0: the 0.25° × 0.25°, daily DOISST v2.0 is resampled to 1° × 1°, monthly data and then co-located with the individual fCO_{2w} measurements in SOCAT (Goddijn-Murphy et al., 2015).

Dataset S1 (Separate file: Flux corrections with different methods. xlsx): Air-sea CO_2 flux corrections using different methods. Lines 2–5 represent the flux corrections for different years using bias_buoy, bias_OI, Fairall96, and Donlon02 temperature corrections, respectively. Lines 7–10 correspond to the flux corrections for different latitude bins using bias_buoy, bias_OI, Fairall96, and Donlon02 temperature corrections, respectively. For example, latitude -89.5 represent the median latitude of the latitude bin [-90, -89] and the corresponding flux correction represent the accumulated flux in this latitude bin.

SI References

Bakker, D. C. E., Bange, H. W., Gruber, N., Johannessen, T., Upstill-Goddard, R. C., Borges, A. V, et al. (2014). Air-sea interactions of natural long-lived greenhouse gases (CO_2, N_2O, CH_4) in a changing climate. In P. S. Liss & M. T. Johnson (Eds.), *Ocean-atmosphere interactions of gases and particles* (pp. 113–169). Berlin, Heidelberg: Springer Berlin Heidelberg. https://doi.org/10.1007/978-3-642-25643-1_3

Bakker, D. C. E., Pfeil, B., Landa, C. S., Metzl, N., O'Brien, K. M., Olsen, A., et al. (2016). A multi-decade record of high-quality fCO_2 data in version 3 of the Surface Ocean CO_2 Atlas (SOCAT). *Earth System Science Data*, *8*(2), 383–413. https://doi.org/10.5194/essd-8-383-2016

Banzon, V., Smith, T. M., Mike Chin, T., Liu, C., & Hankins, W. (2016). A long-term record of blended satellite and in situ sea-surface temperature for climate monitoring, modeling and environmental studies. *Earth System Science Data*, *8*(1), 165–176. https://doi.org/10.5194/essd-8-165-2016

Denvil-Sommer, A., Gehlen, M., Vrac, M., & Mejia, C. (2019). LSCE-FFNN-v1: a two-step neural network model for the reconstruction of surface ocean pCO_2 over the global ocean. *Geoscientific Model Development*, *12*(5), 2091–2105. https://doi.org/10.5194/gmd-12-2091-2019

Fay, A. R., Gregor, L., Landschützer, P., McKinley, G. A., Gruber, N., Gehlen, M., et al. (2021). SeaFlux: Harmonization of air-sea CO_2 fluxes from surface pCO_2 data products using a standardized approach. *Earth System Science Data*, *13*(10), 4693–4710. https://doi.org/10.5194/essd-13-4693-2021

Freeman, E., Woodruff, S. D., Worley, S. J., Lubker, S. J., Kent, E. C., Angel, W. E., et al. (2017). ICOADS Release 3.0: a major update to the historical marine climate record. *International Journal of*

Climatology, *37*(5), 2211–2232. https://doi.org/10.1002/joc.4775

Goddijn-Murphy, L. M., Woolf, D. K., Land, P. E., Shutler, J. D., & Donlon, C. (2015). The OceanFlux Greenhouse Gases methodology for deriving a sea surface climatology of CO_2 fugacity in support of air-sea gas flux studies. *Ocean Science*, *11*(4), 519–541. https://doi.org/10.5194/os-11-519-2015

Gregor, L., Lebehot, A. D., Kok, S., & Scheel Monteiro, P. M. (2019). A comparative assessment of the uncertainties of global surface ocean CO_2 estimates using a machine-learning ensemble (CSIR-ML6 version 2019a)-Have we hit the wall? *Geoscientific Model Development*, *12*(12), 5113–5136. https://doi.org/10.5194/gmd-12-5113-2019

Guinehut, S., Dhomps, A. L., Larnicol, G., & Le Traon, P. Y. (2012). High resolution 3-D temperature and salinity fields derived from in situ and satellite observations. *Ocean Science*, *8*(5), 845–857. https://doi.org/10.5194/os-8-845-2012

Huang, B., Thorne, P. W., Banzon, V. F., Boyer, T., Chepurin, G., Lawrimore, J. H., et al. (2017). Extended reconstructed sea surface temperature, version 5 (ERSSTv5): Upgrades, validations, and intercomparisons. *Journal of Climate*, *30*(20), 8179–8205. https://doi.org/10.1175/JCLI-D-16-0836.1

Huang, B., Liu, C., Banzon, V., Freeman, E., Graham, G., Hankins, B., et al. (2021). Improvements of the daily optimum interpolation sea surface temperature (DOISST) version 2.1. *Journal of Climate*, *34*(8), 2923–2939. https://doi.org/10.1175/JCLI-D-20-0166.1

Iida, Y., Takatani, Y., Kojima, A., & Ishii, M. (2021). Global trends of ocean CO_2 sink and ocean acidification: an observation-based reconstruction of surface ocean inorganic carbon variables. *Journal of Oceanography*, *77*(2), 323–358. https://doi.org/10.1007/s10872-020-00571-5

Jähne, B. (2009). Air-sea gas exchange. *Elements of Physical Oceanography: A Derivative of the Encyclopedia of Ocean Sciences*, 160–169. https://doi.org/10.1016/B978-0-12-409548-9.11613-6

Johnson, K. S. (1982). Carbon dioxide hydration and dehydration kinetics in seawater. *Limnology and Oceanography*, *27*(5), 849–855. https://doi.org/10.4319/lo.1982.27.5.0849

Kennedy, J. J., Rayner, N. A., Smith, R. O., Parker, D. E., & Saunby, M. (2011). Reassessing biases and other uncertainties in sea surface temperature observations measured in situ since 1850: 2. Biases and homogenization. *Journal of Geophysical Research*, *116*(D14), 1–22. https://doi.org/10.1029/2010jd015220

Kennedy, J. J., Rayner, N. A., Atkinson, C. P., & Killick, R. E. (2019). An ensemble data set of sea surface temperature change from 1850: The Met Office Hadley Centre HadSST.4.0.0.0 data set. *Journal of Geophysical Research: Atmospheres*, *124*(14), 7719–7763. https://doi.org/10.1029/2018JD029867

Landschützer, P., Gruber, N., Bakker, D. C. E., Schuster, U., Nakaoka, S., Payne, M. R., et al. (2013). A neural network-based estimate of the seasonal to inter-annual variability of the Atlantic Ocean carbon sink. *Biogeosciences*, *10*(11), 7793–7815. https://doi.org/10.5194/bg-10-7793-2013

Landschützer, P., Gruber, N., & Bakker, D. C. E. (2016). Decadal variations and trends of the global ocean carbon sink. *Global Biogeochemical Cycles*, *30*(10), 1396–1417. https://doi.org/10.1002/2015GB005359

Merchant, C. J., & Embury, O. (2020). Adjusting for desert-dust-related biases in a climate data record of sea surface temperature. *Remote Sensing*, *12*(16), 1–15. https://doi.org/10.3390/RS12162554

Merchant, C. J., Embury, O., Bulgin, C. E., Block, T., Corlett, G. K., Fiedler, E., et al. (2019). Satellite-based time-series of sea-surface temperature since 1981 for climate applications. *Scientific Data*, *6*(1), 1–18. https://doi.org/10.1038/s41597-019-0236-x

Pierrot, D., Neill, C., Sullivan, K., Castle, R., Wanninkhof, R., Lüger, H., et al. (2009). Recommendations for autonomous underway pCO_2 measuring systems and data-reduction routines. *Deep-Sea Research Part II: Topical Studies in Oceanography*, *56*(8–10), 512–522. https://doi.org/10.1016/j.dsr2.2008.12.005

Rayner, N. A., Parker, D. E., Horton, E. B., Folland, C. K., Alexander, L. V., Rowell, D. P., et al. (2003). Global analyses of sea surface temperature, sea ice, and night marine air temperature since the late nineteenth century. *Journal of Geophysical Research: Atmospheres*, *108*(14). https://doi.org/10.1029/2002jd002670

Reynolds, R. W., & Chelton, D. B. (2010). Comparisons of daily Sea surface temperature analyses for 2007-08. *Journal of Climate*, *23*(13), 3545–3562. https://doi.org/10.1175/2010JCLI3294.1

Reynolds, R. W., Rayner, N. A., Smith, T. M., Stokes, D. C., & Wang, W. (2002). An improved in situ and satellite SST analysis for climate. *Journal of Climate*, *15*(13), 1609–1625. https://doi.org/10.1175/1520-0442(2002)015<1609:AIISAS>2.0.CO;2

Reynolds, R. W., Smith, T. M., Liu, C., Chelton, D. B., Casey, K. S., & Schlax, M. G. (2007). Daily high-resolution-blended analyses for sea surface temperature. *Journal of Climate*, *20*(22), 5473–5496. https://doi.org/10.1175/2007JCLI1824.1

Rödenbeck, C., Keeling, R. F., Bakker, D. C. E., Metzl, N., Olsen, A., Sabine, C., & Heimann, M. (2013). Global surface-ocean pCO_2 and sea-Air CO_2 flux variability from an observation-driven ocean mixed-layer scheme. *Ocean Science*, *9*(2), 193–216. https://doi.org/10.5194/os-9-193-2013

Sakurai, T., Yukio, K., & Kuragano, T. (2005). Merged satellite and in-situ data global daily SST. In *Proceedings. 2005 IEEE International Geoscience and Remote Sensing Symposium, 2005. IGARSS'05.* (Vol. 4, pp. 2606–2608). IEEE.

Takahashi, T., Sutherland, S. C., & Kozyr, A. (2008). Global ocean surface water partial pressure of CO_2 database: Measurements performed during 1968-2006 (Version 1.0). *ORNL/CDIAC-152, NDP-088. Carbon Dioxide Information Analysis Center, Oak Ridge National Laboratory, US Department of Energy, Oak Ridge, TN*, *37831*, 20.

Takahashi, T., Sutherland, S. C., Wanninkhof, R., Sweeney, C., Feely, R. A., Chipman, D. W., et al. (2009). Climatological mean and decadal change in surface ocean pCO_2, and net sea-air CO_2 flux over the global oceans. *Deep Sea Research Part II: Topical Studies in Oceanography*, *56*(8–10), 554–577. https://doi.org/10.1016/J.DSR2.2008.12.009

Watson, A. J., Schuster, U., Shutler, J. D., Holding, T., Ashton, I. G. C., Landschützer, P., et al. (2020). Revised estimates of ocean-atmosphere CO_2 flux are consistent with ocean carbon inventory. *Nature Communications*, *11*(1), 1–6. https://doi.org/10.1038/s41467-020-18203-3

Weiss, R. F. (1974). Carbon dioxide in water and seawater: the solubility of a non-ideal gas. *Marine Chemistry*, *2*(3), 203–215. https://doi.org/10.1016/0304-4203(74)90015-2

Xu, F., & Ignatov, A. (2014). In situ SST quality monitor (i Quam). *Journal of Atmospheric and Oceanic Technology*, *31*(1), 164–180. https://doi.org/10.1175/JTECH-D-13-00121.1

Yang, C., Leonelli, F. E., Marullo, S., Artale, V., Beggs, H., Nardelli, B. B., et al. (2021). Sea surface temperature intercomparison in the framework of the copernicus climate change service (C3S). *Journal of Climate*, *34*(13), 5257–5283. https://doi.org/10.1175/JCLI-D-20-0793.1

Yu, L., & Weller, R. A. (2007). Objectively analyzed air–sea heat fluxes for the global ice-free oceans (1981–2005). *Bulletin of the American Meteorological Society*, *88*(4), 527–540. https://doi.org/10.1175/BAMS-88-4-527

Zeebe, R. E., & Wolf-Gladrow, D. (2001). *CO_2 in seawater: equilibrium, kinetics, isotopes*. Elsevier Science, pp. 85–140.

Zeng, J., Nojiri, Y., Landschützer, P., Telszewski, M., & Nakaoka, S. (2014). A global surface ocean fCO_2 climatology based on a feed-forward neural network. *Journal of Atmospheric and Oceanic Technology*, *31*(8), 1838–1849. https://doi.org/10.1175/JTECH-D-13-00137.1